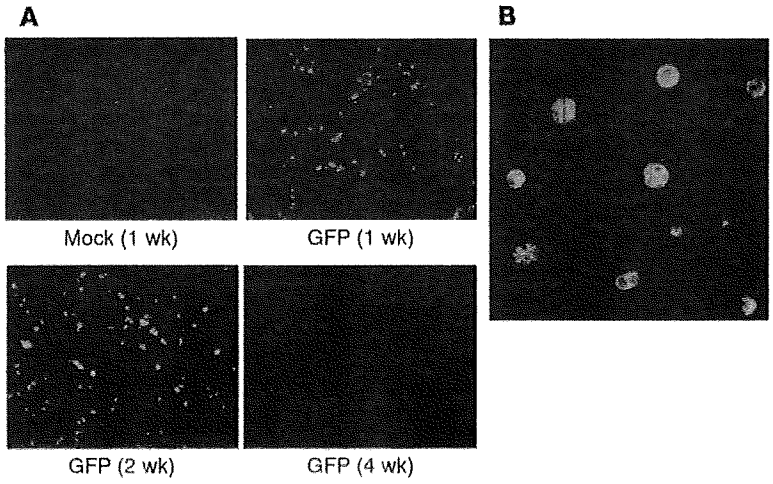

Figure 2
Development of local gene-delivery system that is capable of targeting colon. (**A**) A complex of mock or enhanced GFP vector with DOTAP/enhancer reagent was locally microinjected into the proximal part (just below ileocecal junction) of colon of TCRαKO mice thorough the laparotomy approach. The mice were sacrificed 1, 2, or 4 weeks after the microinjection. Frozen sections of the injection site were subjected to fluorescent microscopic analysis for the detection of GFP signals. The result is representative of 6 individual experiments. (**B**) Adherent cell populations (such as macrophages and fibroblasts) were isolated from the deepithelialized mucosa with GFP vector delivery using a "walk-out" approach. The obtained cells with an adherent ability were subjected to fluorescent microscopic analysis for the detection of GFP signals. Original magnification, ×40.

in several human epithelial cancer cell lines in vitro (9). This was further confirmed here (Supplemental Figure 3). To determine whether IL-22 activates these signaling cascades in normal CECs, we isolated fresh CECs as crypt units from mice by using the previously validated EDTA perfusion (30 mM) method (21) and stimulated them with IL-22. Similar to human cancer cell lines, IL-22 dose dependently activated STAT3 in the freshly isolated CECs from mice (Figure 1F). In contrast, IL-22 failed to activate the ERK1/2 cascade in the freshly isolated CECs (Figure 1F). To determine whether similar effects were observed in humans, surgically resected human colonic specimens with histologically normal appearance were subjected to organ culture with 5 ng/ml of IL-22. Notably, Western blot analysis showed that STAT3 activation in the colonic specimens was significantly enhanced by stimulation with IL-22 (Figure 1G). In contrast, IL-22 did not enhance the activation of ERK1/2 in the colonic specimens (Figure 1G). Accumulation of phospho-STAT3 in the nucleus of CECs within the IL-22–stimulated human specimens was confirmed by immunohistochemical analysis (Figure 1H). These findings suggest that IL-22 specifically activates STAT3 but not ERK1/2 in normal mouse and human CECs (without neoplastic changes) and are consistent with recent reports showing an inability of IL-22 to activate ERK1/2 in keratinocytes and hepatocytes (10, 17).

Establishment of local gene-delivery approach capable of specifically targeting a selected region within the intestine. Microbial mediated in vivo gene-delivery systems using adenovirus or *Lactococcus lactis* have been used to cause local overexpression of some regulatory molecules in the intestine (22, 23). However, it may be difficult to avoid certain risks in these approaches, e.g., unwanted immune stimulation by virus-like particles or expression of genes of interest throughout the entire intestine by enteric bacteria–mediated gene delivery. To minimize such risks, we tested the efficacy of non-microbial-mediated gene-delivery systems using different agents (e.g., In Vivo GeneSHUTTLE, in vivo MegaFectin, in vivo-jetPEI, TransIT-In Vivo, Chariot, Lipofectamine 2000, and Cellfectin) and different routes for delivery (i.v., intrarectal, and direct microinjection). As a result, we discovered that a pressurized local microinjection of vector/cationic lipid (1,2-dioleoyl-3-trimethylammonium propane-cholesterol [DOTAP-cholesterol])/DNA-condensing agent–2 complexes with 20 mM HEPES (24–26) directly into the colonic mucosa could efficiently deliver the gene of interest (enhanced GFP) into the injected site. As shown in Figure 2A, large numbers of GFP^+ cells could be detected in the colonic LP but not CECs within 1 week after gene delivery by this method. GFP signals were detectable in an adherent cell population that was obtained from the deepithelialized mucosa using a "walk-out" approach (27) (Figure 2B). In contrast, GFP signals were not detected in T or B cells (data not shown). Interestingly, few GFP^+ cells were detectable in the mesenteric lymph nodes and spleen (data not shown). The GFP signal in the colonic LP became undetectable 4 weeks after delivery (Figure 2A). These observations show that inducible gene expression by the method of local gene-delivery system is transient (presumably due to utilization of circularized but not linear DNA) and restricted to the colon. Adherent cell populations such as fibroblasts and macrophages may be the major targets of this in vivo gene-delivery system.

Rapid attenuation of Th2-mediated colitis by local IL-22 gene delivery. IL-22 expression was significantly lower in UC and TCRαKO mice as compared with CD and CD45RB models (8, 11) (Figure 1). We therefore determined whether supplementation of IL-22 expression through our local gene-delivery system contributed to the attenuation or exacerbation of chronic colitis in TCRαKO mice. To do so, lipid complexes with secretion vector carrying full-length mouse IL-22 cDNA or mock vector were injected into the proximal colon (just below the ileocecal junction) of TCRαKO mice selected for the presence of severe colitis as defined by enlarged colonic diameter, as previously described (28) (Figure 3C). These mice were sacrificed 2 weeks after local gene delivery. Local gene delivery of IL-22 but not the mock vector induced a marked increase in IL-22 expression in the injection site within the proximal colon (Figure 3A). In contrast, IL-22 expression in the noninjection site (distal colon) was not affected by local gene delivery (Figure 3A). In addition, local gene delivery of IL-22 vector significantly enhanced STAT3 activation in the CECs of proximal colon (the injected site) but not distal colon (noninjected site) as defined by the levels of phospho-STAT3 (Figure 3B and data not shown). Of note, IL-22 gene delivery led to "prompt" attenuation of colitis at the injection but not the noninjection site, as indicated by a significant reduction in the colonic diameter within 2 weeks after IL-22 gene delivery (Figure 3, C and D). This finding was further confirmed by histological analysis that showed the significant reduction of colonic thicknesses and disease scores in the region where IL-22 gene delivery was performed (Figure 3, E and F).

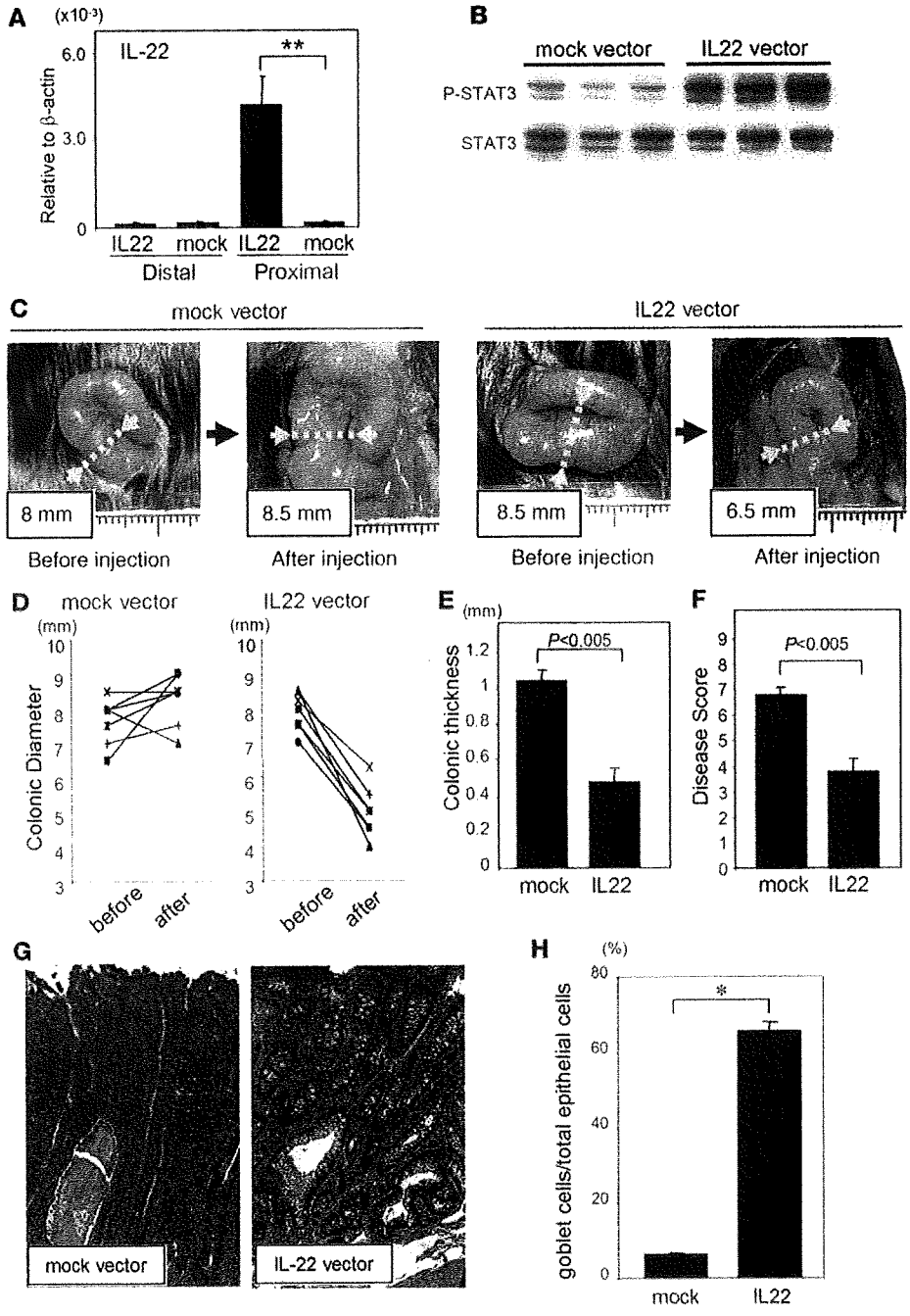

Figure 3

Rapid attenuation of colitis by local IL-22 gene delivery. (**A** and **B**) Complexes of IL-22 secretion or mock vector with DOTAP/enhancer reagent were microinjected into the proximal part of colon of TCRαKO mice with colitis. Expressions of IL-22 in the noninjected distal part and injected proximal part are shown in **A**. Results represent the averages ± SEM (n = 6–7). $^{**}P < 0.005$. Protein lysates from the CECs of the proximal part of colon with mock or IL-22 gene delivery were subjected to immunoblot for evaluation of STAT3 activation (**B**). (**C–H**) Laparotomy was carried out on anesthetized TCRαKO mice (24 weeks of age) to confirm the presence of severe colitis as indicated by a marked enlargement of colonic diameter (before injection). Local gene delivery of IL-22 or mock vector into the proximal part (just below the ileocecal junction) was performed in selected TCRαKO mice (n = 7 each group) that had severe colitis. Mice were sacrificed 2 weeks after microinjection. IL-22 gene delivery attenuated the inflammation at the injection sites; colonic diameter at the injection sites was markedly reduced in TCRαKO mice that received IL-22 (**C**, right panels) but not mock (**C**, left panels) vector delivery. Results are summarized in **D**. Colonic thickness (**E**) and disease score (**F**), which were evaluated by histological examination (n = 6–7), are shown. Histology of the proximal colon where gene delivery with mock (left panel) or IL-22 vector (right panel) was received are shown in **G**. Original magnification, ×10. (**H**) Percentages of goblet cells among total epithelial cells within the colon where mock (n = 6) or IL-22 (n = 6) vector delivery were received are shown. $^{*}P < 0.001$.

Goblet cell depletion, which is prominently observed in UC in comparison with CD (12, 29, 30), was observed in the diseased colon of TCRαKO mice treated with mock vector (Figure 3G). Interestingly, IL-22 gene delivery induced a significant restoration of goblet cell expression in TCRαKO mice (Figure 3, G and H). These data suggest that IL-22 contributes to rapid amelioration of chronic colitis in association with goblet cell restitution in TCRαKO mice.

Induction of STAT3-mediated mucus-associated protein expression by IL-22. Supplementation of IL-22 expression in the inflamed colon of TCRαKO mice by local gene delivery significantly reverted goblet cell depletion typically observed in TCRαKO mice (Figure 3, E and F). Therefore, to determine whether IL-22 possesses an ability to directly stimulate goblet cells, the expression of goblet cell–associated genes in freshly isolated CECs from WT mice without colitis was examined after IL-22 gene delivery. Interestingly, real-time PCR analysis showed that inducible IL-22 overexpression stimulated CECs to express MUC1, -3, -10, and -13, which are involved in mucus layer formation (Figure 4A). Western blot analysis further confirmed that STAT3 activation as well as MUC1 production in WT CECs was induced by local gene delivery of the IL-22–encoding but not mock vector (Figure 4B). In addition, like mouse CECs, IL-22 enhanced the expression of MUC1, -3, and -13 in a human T84 CEC line (Figure 4C). Western blot analysis confirmed that MUC1 production was enhanced after stimulation of T84 cells

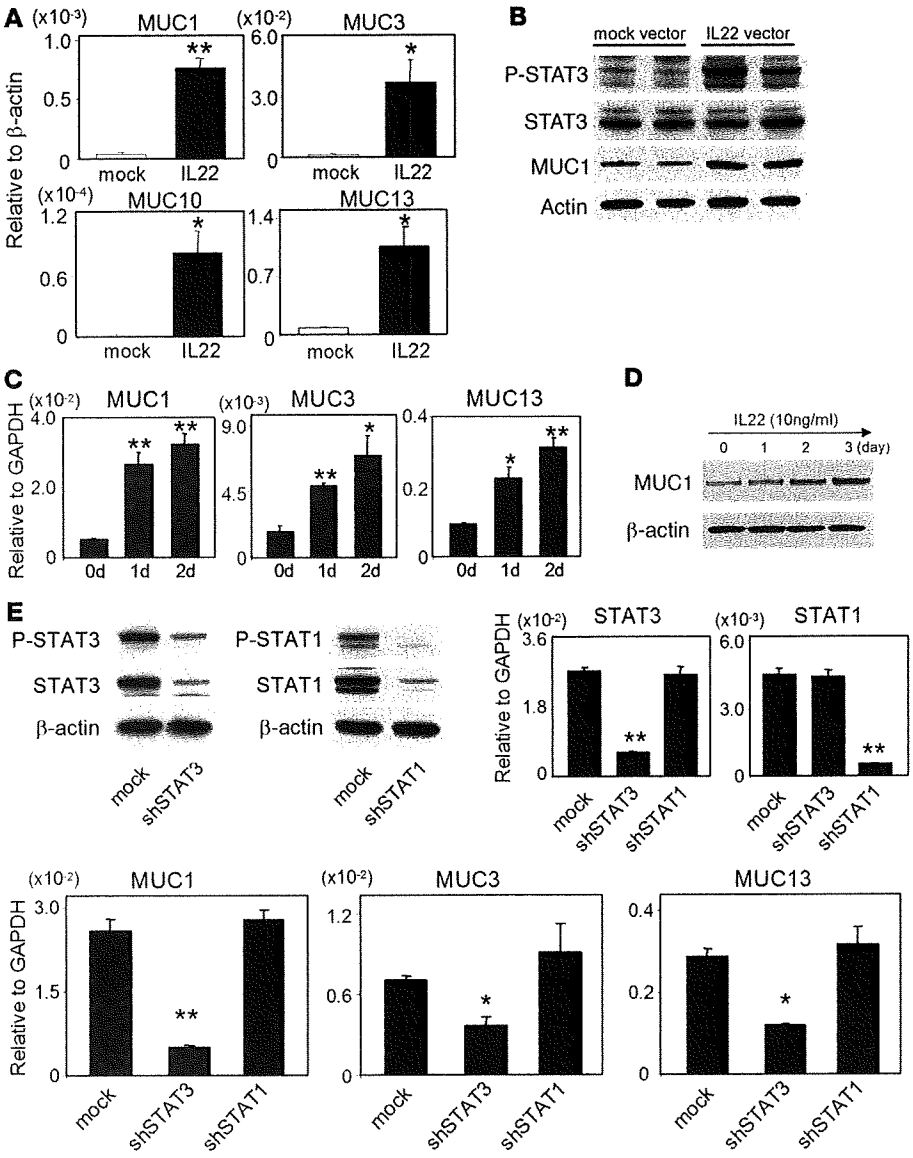

Figure 4

IL-22–mediated induction of a series of Muc expressions in CECs through STAT3 activation. (**A** and **B**) CECs were freshly isolated from WT mice that had received local gene delivery of mock (white bars, $n = 5$) or IL-22 secretion (black bars, $n = 5$) vector into the proximal colon. Expressions of MUCs by CECs are shown in **A**. Protein lysates from freshly isolated CECs were subjected to immunoblot with anti–phospho-STAT3 (P-STAT3) or anti-MUC1 (MUC1) Abs (**B**). After stripping the Abs, the membrane was reprobed with anti-STAT3 (STAT3) or actin Abs. (**C** and **D**) Average expressions of MUCs by T84 cells stimulated with IL-22 (10 ng/ml) in duplicates of 3 individual experiments are shown in **C**. Protein lysates were immunoblotted with anti-MUC1 Abs (**D**). After stripping the Abs, membrane was reprobed with β-actin Abs. (**E**) T84 cells were transfected with a combination of STAT3 shRNA vectors (pKD-STAT3-v2 and -v3) or STAT1 shRNA vectors (pKD-STAT1-v1 and -v2) using Amaxa, which has been shown to efficiently transfect the gene of interest into cells resistant to typical transfection approaches. Cell line with mock vector transfection was used as control. After stimulation of the shRNA- or mock vector–transfected cells with IL-22 (10 ng/ml), the efficiency of the combined shRNA on the silencing of STAT3 or STAT1 expression was confirmed by Western blot (upper left panels) and real-time PCR analyses (upper right panels). Expression of MUC1, -3, and -13 by shRNA (STAT3 or STAT1) or mock vector–transfected cells stimulated with IL-22 was evaluated by real-time PCR analysis. Data represent the average of 3 individual experiments. $^{**}P < 0.005$; $^{*}P < 0.05$.

with IL-22 in a time-dependent manner (Figure 4D). To determine whether STAT3 is required for the IL-22–mediated enhancement of mucus-associated protein (Muc) production, we initially optimized the conditions in order to sufficiently inhibit STAT3 expression in the T84 cell line by employing a Nucleofector approach to introduce combined STAT3-shRNA vectors. Inhibition of STAT3 resulted in a significant decrease in IL-22–mediated MUC1, -3, and -13 expression by the T84 cell line (Figure 4E). A capability of IL-22 to stimulate STAT1 activity has previously been demonstrated (17). Therefore, we next tested to determine whether STAT1 is involved in the IL-22–mediated production of MUCs. However, inhibition of STAT1 did not affect MUC production by the T84 cells line (Figure 4E). These findings identify IL-22 as a unique cytokine capable of enhancing mucin production by CECs through the activation of STAT3. Indeed, STAT3 has been demonstrated to interact with a promoter region within the MUC1 gene (31).

The major Th17 cytokine IL-17A has previously been demonstrated to stimulate airway epithelial cells to produce Muc5 (32). Therefore, to determine whether, similarly to IL-22, IL-17 is also involved in Muc production in the intestine, gene delivery of IL-17A was performed in the colon of WT mice. However, gene delivery did not enhance the activation of STAT3 or the expression of Muc1, -3, -10, or -13 in CECs (Supplemental Figure 4). In addition, Muc5 was undetectable in CECs. These findings suggest the physiologically different functions of IL-22 versus IL-17 in the intestine.

Enhanced mucus production plays a crucial role in IL-22–mediated amelioration of chronic colitis in TCRαKO mice. Since Muc family members form a static external barrier along the epithelial cell surface (33, 34), we determined whether the rapid attenuation of chronic colitis induced by supplementation of IL-22 expression was mediated by the enhanced Muc expression observed. To do so, IL-22 gene delivery was performed in the inflamed colons of TCRαKO mice with or without mucolytic treatment to remove colonic mucus layer. For the mucolytic treatment, a mucolytic agent, *N*-acetyl-L-cystein (20 μg/h), was continuously supplied for 14 days in the colonic lumen through a catheter connected to an ALZET osmotic

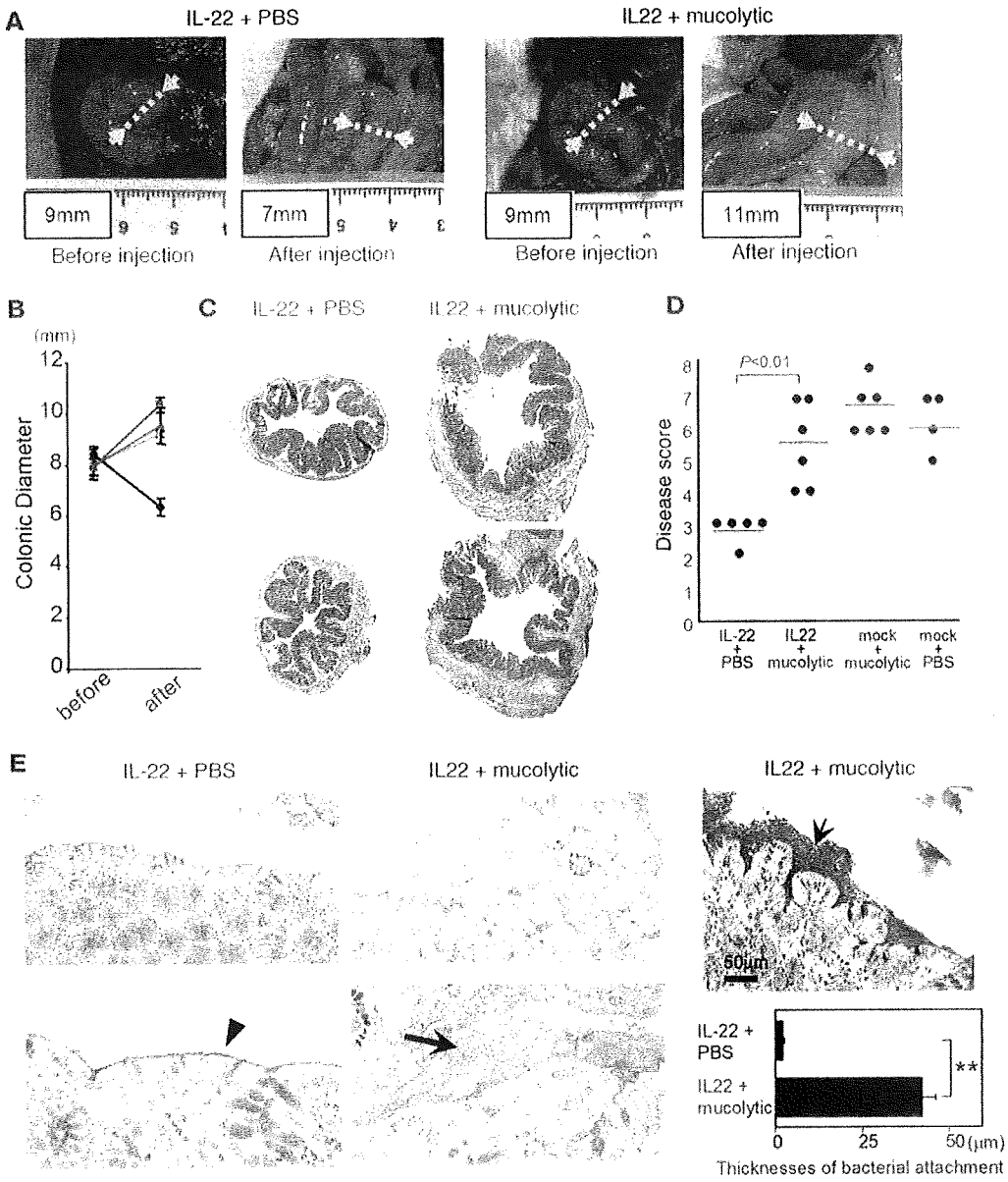

Figure 5

Enhanced mucus production mediates IL-22–induced rapid attenuation of UC-like disease. (**A**–**D**) Laparotomy was carried out on anesthetized TCRαKO mice (24 weeks of age) to confirm the presence of colitis as indicated by a marked enlargement of colonic diameter (**A**, before injection). Local gene delivery of IL-22 vector into the proximal part (just below the ileocecal junction) was performed in the diseased TCRαKO mice. PBS (**A**, left panels) or mucolytic agent (**A**, right panels) was continuously administered into the cecal lumen through osmotic pump for 2 weeks. The mice were sacrificed 2 weeks after the microinjection (**A**, after injection). Numbers in panels indicate the colonic diameter. Summary of change in colonic diameter of 4 mouse groups (n = 4–6) (IL-22 gene delivery plus PBS treatment, black; IL-22 gene delivery plus mucolytic treatment, red; mock gene delivery plus mucolytic treatment, blue; and mock gene delivery plus PBS treatment, green) is shown in **B**. Histology of the colon from IL-22–gene–delivered TCRαKO mice with PBS (**C**, left panels) or mucolytic agent (**C**, right panels) and summarized disease score (**D**) are shown. (**E**) Alcian blue staining shows preserved mucus layer (blue liner, arrowhead) along epithelial surface of IL-22–gene–delivered TCRαKO mice (left panels). In contrast, mucolytic treatment impaired the mucus layer formation with significant adhesion of enteric bacteria (arrow; middle panels). Adhesion of enteric bacteria was confirmed by toluidine blue staining (top right panel, arrow). Average (randomly selected 20 fields/each mouse of 4 mice) of thicknesses of bacterial layer attached to epithelial surface is summarized in bottom right panel. $^{**}P < 0.001$. Original magnification, ×1 (**C**); ×10 (**E**, top left panels); ×40 (**E**, bottom left panels).

pump that was implanted within the dorsa of mice. The dose used has been optimized so as not to induce systemic side effects (35). Interestingly, local IL-22 gene delivery failed to attenuate the colitis (as judged by colonic diameter) in TCRαKO mice that were treated with the mucolytic agent (Figure 5, A and B). Histological examination confirmed that TCRαKO mice that received IL-22 gene delivery plus mucolytic treatment in fact developed more severe colitis compared with mice that received IL-22 gene delivery plus

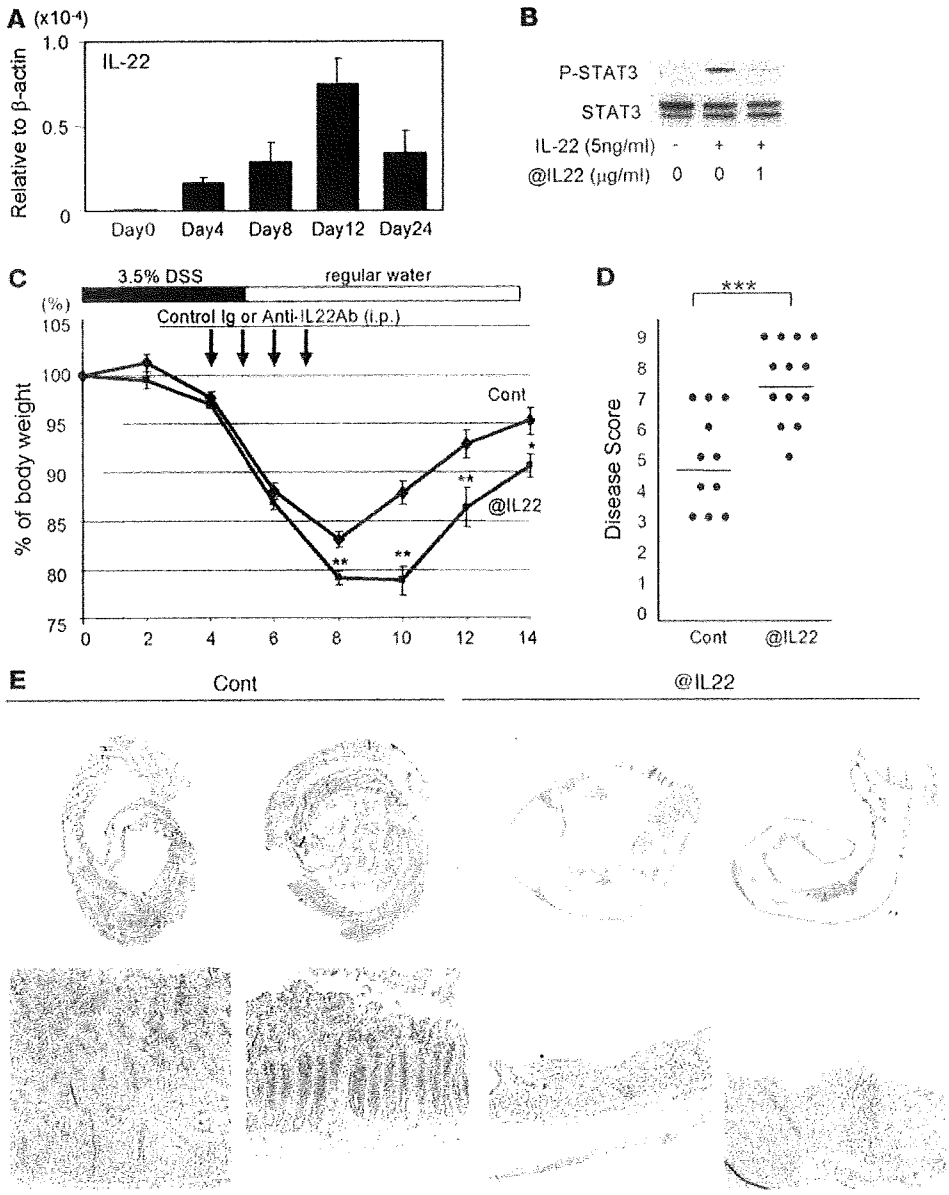

Figure 6

Role of IL-22 in the restitution of goblet cells during recovery from acute intestinal injury. (**A**) DSS was administered into WT mice for 5 days and the treatment terminated to induce recovery phase. Expression levels of IL-22 (ratio of IL-22/β-actin) in the colonic LP at days 0 (normal), 4 (acute phase), 8, 12 (recovery phases), and 24 are shown (n = 4 each group). (**B**) CECs were freshly isolated as crypt units from WT mice and stimulated with IL-22 (5 ng/ml) in the presence or absence of anti–IL-22 Abs. Protein lysates (10 μg) from the stimulated CECs were subjected to immunoblot with anti–phospho-STAT3 (P-STAT3) Abs. After stripping Abs, the membrane was reprobed with anti-STAT3 Abs (STAT3). (**C–E**) WT mice were treated with 3.5% DSS in drinking water for 5 days. Repeated i.p. administration of 1.5 mg/injection of anti–IL-22 Abs (@IL22; n = 12) or control Ig (Cont; n = 12) was performed at days 4, 5, 6, and 7 in selected mice that showed similar body weight loss at day 4 as compared with initial body weight. Body weight change (**C**), "Swiss rolls" (**D**, upper panels), and high magnification (**D**, bottom panels) of colons stained with Alcian blue are shown. $^{*}P < 0.05$; $^{**}P < 0.005$; $^{***}P < 0.001$. Original magnification, ×1 (**E**, top row); ×20 (**E**, bottom row). Disease scores are summarized in **E**.

mock treatment (Figure 5, C and D). Notably, a preserved mucus layer, as evaluated by Alcian blue staining, was detectable along the surface of the colonic epithelium in TCRαKO mice that received IL-22 gene delivery (Figure 5E). In contrast, mucolytic treatment significantly impaired the structure and expression of the mucus layer (Figure 5E). Interestingly, the impaired mucus layer was associated with markedly enhanced adhesion of enteric bacteria to the epithelial cell surface (Figure 5E). These findings suggest that the increased production of Muc, which contributes to preserve mucus layer formation, is involved in the rapid attenuation of established chronic colitis in TCRαKO mice, which is mediated by IL-22.

Contribution of IL-22 to facilitate goblet cell restitution in intestinal inflammation. A useful model to study disease-associated CEC homeostasis is the dextran sulfate sodium–induced (DSS-induced) colitis model, in which acute intestinal inflammation with epithelial loss is induced by treatment with DSS. After termination of the DSS treatment, the acute colitis spontaneously recovers, with marked CEC regeneration with goblet cell restitution (21). Interestingly, we observed that IL-22 expression in the colon was significantly upregulated during the recovery phase (after termination of DSS treatment) of DSS colitis (Figure 6A). Therefore, to study the role of IL-22 in this colitis model, we neutralized IL-22 activity in vivo during the recovery phase by administering anti–IL-22 Abs that recognize a binding site within IL-22 to IL-10R2 (36) and are indeed capable of inhibiting IL-22–induced activation of STAT3 in CECs (Figure 6B).

Treatment with the anti–IL-22 Abs significantly delayed the recovery from DSS-induced acute colitis as judged by body weight loss (Figure 6C), a widely used measure of injury in DSS colitis (37). In addition, histological analysis using "Swiss rolls" of entire colon showed that the anti–IL-22–treated group exhibited thin colonic wall as compared with the control IgG-treated group (Figure 6D). Interestingly, a strong accumulation of goblet cells, which is generally associated with regeneration of CECs during the recovery phase

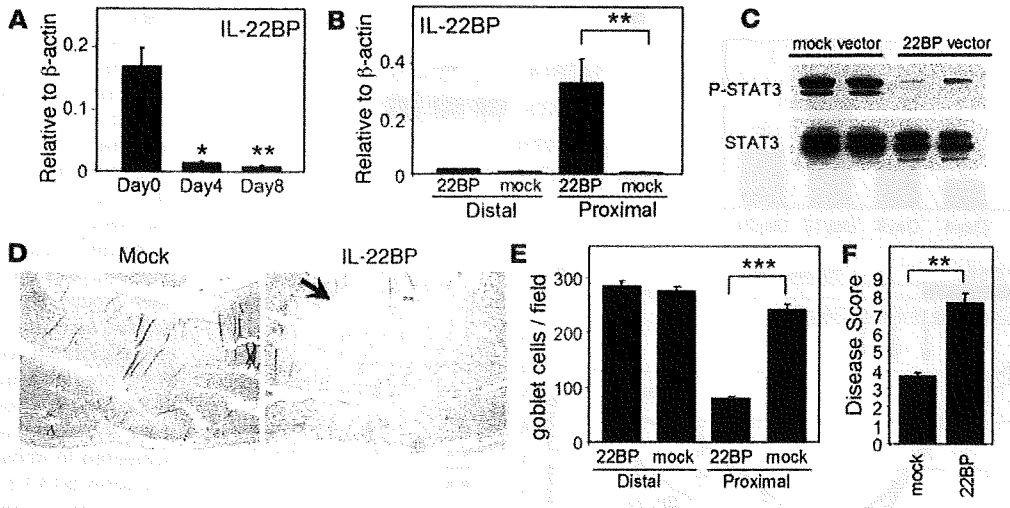

Figure 7

Effect of IL-22BP on the suppression of IL-22 activity in vivo. (**A**) Expression levels of IL-22BP (ratio of IL-22BP/β-actin) in the colonic LP at days 0 (normal), 4 (acute phase), and 8 (recovery phase) of DSS colitis are shown. (**B–F**) Local IL-22BP gene delivery was performed in the proximal part of the colon, and the mice were subsequently treated with 3% DSS on the third day after the delivery. DSS treatment was terminated at day 5 after initiation, and mice were sacrificed at day 8. Expression of IL-22BP in the distal (noninjected site) and proximal (injected site) colons of mice with mock or IL-22BP gene delivery is shown (**B**). CECs were freshly isolated from DSS-treated WT mice that had received local gene delivery of mock or IL-22BP vector in the proximal colon. Protein lysates from the freshly isolated CECs were subjected to immunoblot with anti–phospho-STAT3 Abs (**C**). After stripping the Abs, the membrane was reprobed with anti-STAT3 Abs (**C**). The proximal colon of mock (left panel) or IL-22BP (right panel) gene–delivered mice was subjected to Alcian blue staining (**D**). Significant reduction of goblet cells (blue) is observed in the colon of IL-22BP–delivered mice as compared with that of mock-delivered mice. Ulceration is indicated by arrow. Original magnification, ×4. Averages of goblet cells/field in the noninjected (distal colon) and injected (proximal colon) site are shown in **E**. Disease score in the proximal colon (injected site) is summarized in **F**. $^*P < 0.05$; $^{**}P < 0.005$; $^{***}P < 0.001$.

of DSS colitis, was observed in the control Ab-treated group but not the anti–IL-22 Ab–treated group (Figure 6D). In addition, intestinal injury as judged by disease scores was exacerbated in the anti–IL-22 Ab–treated group (Figure 6E). These findings suggest that IL-22 contributes to inflammation-associated goblet cell restitution.

Suppression of IL-22–mediated goblet cell restitution by IL-22–binding protein. IL-22–binding protein (IL-22BP) has been demonstrated to sufficiently neutralize IL-22 activity in vitro (38). Interestingly, expression of colonic IL-22BP was significantly downregulated during the recovery phase of DSS colitis (Figure 7A) at a time when IL-22 was upregulated (Figure 6A). Therefore, to further confirm an involvement of IL-22 in goblet cell restitution, local delivery of lipid complexes with secretion vector carrying a full-length mouse IL-22BP cDNA was performed in the proximal colon of WT mice. The mice were subsequently treated with DSS and then sacrificed 3 days after termination of the DSS treatment. Significantly, enhanced IL-22BP expression was observed in the injected, but not the noninjected, site of the colon (Figure 7B). IL-22BP gene delivery downregulated the activation of STAT3 in CECs within the injected, but not the noninjected, sites of the colon (Figure 7C). Of note, goblet cells were significantly reduced within the injected site of the IL-22BP–delivered group as compared with the mock-delivered group (Figure 7, D and E). In contrast, there was no significant difference in the goblet cell numbers within the noninjected sites among these groups (Figure 7E). Interestingly, ulcerations were recognized in the injected sites of all mice (6 of 6) that received IL-22BP gene delivery and 2 out of 6 mice that received mock delivery (Figure 7D). In addition, the inflammation in the proximal colon (injected site) was significantly exacerbated by IL-22BP gene delivery (Figure 7F). These data suggest that IL-22BP suppresses inflammation-associated goblet cell restitution and recovery from acute intestinal injury by inhibiting IL-22 activity.

Discussion

IL-22 possesses the ability to induce both STAT3-mediated expression of regulatory molecules (7–10) and ERK-mediated expression of proinflammatory molecules (e.g., IL-8) (8, 11). The opposing effects of IL-22 have made it difficult to predict the role of IL-22 in IBD. We herein demonstrate that IL-22 contributes to rapid amelioration of local inflammation associated with a Th2-mediated colitis through activation of STAT3 in CECs. STAT3-mediated activation of acquired immune responses is well known as playing a pathogenic role in colitis by enhancing the survival of pathogenic T cells (37, 39). In contrast, STAT3-mediated activation of innate immune responses contributes to the suppression of colitis, as indicated by the spontaneous development of colitis in mice in which STAT3 is extinguished only in innate cells such as CECs or macrophages (40–42). Since IL-22 specifically targets innate immune pathways (7, 9), selective activation of STAT3 in CECs but not acquired immune cells by IL-22 may contribute to amelioration of chronic Th2-mediated colitis.

IL-22 has previously been demonstrated to stimulate keratinocytes and CEC lines to produce several regulatory molecules, such as IL-10, SOCS3, and antibacterial peptides (β-defensin 2, psoriasin, calgranulins A and B) (7–10). In addition, we herein demonstrate what we believe is a novel function of IL-22. IL-22 contributes to the improvement of colitis-associated mucus layer destruction associated with goblet cell depletion by enhancing the

production of membrane-bound mucins (Muc1, -3, -10, and -13). Membrane-bound mucins form a static external barrier at the epithelial surface and are stored in goblet cell vacuoles (13, 34, 43). Importantly, our studies suggest that the enhanced mucus barrier formation participates in the IL-22–mediated attenuation of Th2-mediated colitis. Indeed, recent studies have indicated that Muc2 and Muc3 contribute to the suppression of experimental colitis (33, 34). In addition, a more recent study clearly demonstrated a critical role of intestinal mucus layer for the suppression of colitis (44). UC, which is characterized by a thin mucin layer in association with goblet cell depletion, exhibits strong expression of Muc2 and Muc4 and low expression of Muc1 and Muc3 (13). Therefore, it is possible that insufficient production of IL-22 may facilitate goblet cell depletion and impair mucus layer formation in UC. Goblet cells specifically produce not only Muc but also other molecules involved in both regulation (e.g., trefoil factor) (45) and exacerbation (e.g., resistan-like β [RELMβ]) (46) of colitis. Interestingly, IL-22 downregulated the expression of goblet cell–derived RELMβ, a potential pathogenic goblet cell product (K. Sugimoto, unpublished observations).

Accumulating data in experimental IBD models have suggested the involvement of both common and distinct mechanisms of pathogenesis in UC versus CD. Experimental chronic UC-like disease is significantly contributed to by Th2 cytokines (14, 18). In contrast, IL-23/IL-17 pathways have recently been shown to play a pathogenic role in experimental CD-like diseases (15, 16, 47, 48). The relevance of the data from experimental colitis models to human CD is supported by recent studies showing a negative association of IL-23 receptor polymorphisms to the development of IBD (49). Interestingly, IL-22, which is preferentially expressed by Th17 cells (4, 5), is significantly increased in CD patients in comparison with UC patients (8, 11). Thus, Th17 cells may be responsible for both deleterious effects through IL-17 production and beneficial effects through IL-22 production through an increase of mucus production. Indeed, a recent study has demonstrated a contribution of the Th17 subset in the suppression of a Th2-mediated asthma model that is characterized by dysregulated mucus production in the trachea (50).

We developed a novel microinjection-based local gene-delivery system that allowed the targeting of inflamed mucosa and supplementation of local IL-22 expression restricted within the delivered site. Microbial-mediated in vivo gene delivery using adenovirus or *L. lactis* has been used to cause local overexpression of some molecules in the intestine (22, 23). However, it may be difficult to avoid certain risks in these approaches, e.g., unwanted immune stimulation by virus-like particles or expression of genes of interest throughout the entire intestine by enteric bacteria–mediated gene delivery. Alternatively, our microinjection-based gene-delivery approach has several advantages. These include the restricted expression of the gene of interest to the injection site, transient expression (less than 4 weeks), and utilization of potentially harmless carriers as compared with microorganisms. Therefore, it is likely that potential side effects are minimized. In humans, such microinjection-based local gene delivery may be performed via endoscopy.

In summary, we provide an unexpected insight into the role of the Th17 cytokine IL-22 in Th2-mediated chronic colitis of TCRαKO mice. IL-22 stimulates mucus production and goblet cell restitution under intestinal inflammatory conditions and also contributes to the rapid attenuation of this inflammation. In addition, we describe a newly established local gene-delivery approach that is capable of targeting inflamed mucosa and may provide a means to developing a new therapeutic strategy for treating mucosal inflammation.

Methods

Reagents. Abs against phosphorylated (Thr202/Tyr204) and total ERK1/2 and phosphorylated STAT3 (Tyr705) (Cell Signaling); anti-STAT3, anti-MUC1, and anti-actin (C-II) Abs (Santa Cruz); anti-human β-actin Abs (Sigma-Aldrich); and HRP goat anti-rabbit and goat anti-mouse secondary Abs (Pierce) were used. Recombinant human IL-22 and recombinant mouse IL-22 were obtained from R&D Systems. Anti–IL-22 Abs that recognize a binding site within IL-22 to IL-10R2 (36) were generated by immunization of rabbits with keyhole limpet hemocyanin–conjugated peptides (VLLPQSDRFQPYMQE-c). The Abs were purified from the immune serum by affinity purification with the peptide used for immunization. The specificity of the Abs was confirmed by Western blot analysis using recombinant mouse IL-22 protein.

Mouse and human materials and disease evaluation. Mice were maintained under specific pathogen–free facilities at Massachusetts General Hospital. All mice used were of the C57BL/6 background. Viable and pure mouse CECs were isolated as crypt units by using an EDTA perfusion method, as previously described (37). Intestinal inflammation in mice was evaluated according to previously described criteria (28, 37). In chronic colitis, the disease score was estimated by a combination of gross score (0, normal appearance; 1, focal change; 2, mild change in entire colon; 3, severe change in entire colon) and histological scores (0–3, inflammatory cell infiltration; 0–3, epithelial cell elongation). In DSS-induced acute intestinal damage, ulceration score (0, no ulceration; 1, presence of erosion; 2, presence of focal ulceration; 3, presence of multiple ulcerations) was used instead of gross score. All experiments were approved by Subcommittee on Research Animal Care of Massachusetts General Hospital. Human colonic tissue samples were obtained from the tissue bank of the Center for the Study of Inflammatory Bowel Disease and Pathology at Massachusetts General Hospital. Caco2, SW480, and T84 cell lines were obtained from ATCC. T84 cells were grown on filter membranes until they formed a confluent polarized monolayer (>1000 $\Omega \cdot cm^2$). Cells were then stimulated with several doses of cytokines from upper or lower compartments.

Gene expression analyses. RNA was extracted from the total mouse colonic LP after removing CECs by the EDTA perfusion method (30 mM), as previously described (21). 10 μg mRNA was subjected to DNA microarray analysis using PGA Mouse v1.0 probe set (19,549 oligos), as previously described (21). For the supplementation of genes that were not included in the gene chips used, large numbers of primer sets for the detection of 1,300 molecules were generated and used for real-time PCR analysis. Real-time PCR was carried out using the SYBR green system (Stratagene), as previously described (37).

Protein and mucus layer analyses. Western blot analysis was performed using the ECL detection system (Amersham), as previously described (37). Paraffin-embedded tissue sections were stained with H&E, Alcian blue, and PAS using standard techniques. For analysis of the mucus layer, Carnoy solution was used for the fixation of tissues to preserve the mucus layer (51). Immunohistochemical staining using frozen tissues was performed as previously described (21).

Gene silencing in vitro. To determine whether STAT3 is required for the IL-22–mediated enhancement of mucus-associated protein production, we initially optimized the conditions in order to sufficiently inhibit STAT3 expression in the T84 cell line by employing a Nucleofector approach to introduce combined STAT3-shRNA vectors. STAT3 knockdown was performed using STAT3 shRNA vectors (pKD-STAT3-v2 and -v3; Upstate). STAT1 knockdown was performed using STAT1 shRNA vectors (pKD-STAT1-v1 and -v2; Upstate). T84 cells were resuspended at 2×10^6 cells/ml

in Cell Line Kit T buffer (VCA-1002; Amaxa Biosystem) and subjected to nucleofection with 2 μg of shRNA or mock vector using Nucleofector (Amaxa) according to the manufacturer's instruction. One day after the transfection, cells were stimulated with 10 ng/ml of IL-22 for 2 days and immediately subjected to protein lysis and RNA extraction.

Local in vivo gene delivery. Full-length mouse IL-22 and IL-17A cDNAs from WT LP cells treated with DSS was amplified by RT-PCR (forward, 5′-CGATCTCTGATGGCTGTCCT, reverse, 5′-ACGCAAGCATTTCTCAGAGA for IL-22; forward, 5′-AACATGAGTCCAGGGACAGC, reverse, 5′-CTGCCTGGCGGACAATCGAG for IL-17A) and cloned into pCR 2.1 TOPO vector (Invitrogen). After digestion with *BamHI* and *XhoI*, cDNA was subcloned into the pIRES-hrGFPII vector (Stratagene) or pSecTag2/Hygro vector (Invitrogen). For in vivo local gene delivery into the colon, DNA/lipid complex was made by the incubation of vectors with cationic lipid (DOTAP-cholesterol) with an enhancer 2 (in vivo MegaFectin reagent; Qbiogene) according to the manufacturer's instructions. After dilution of the lipid/DNA complex with 10 mM HEPES, the complex (20 μg DNA) was directly injected into the proximal colon of mice using a microinjection needle (Harvard Apparatus) through laparotomy. Selected TCRαKO mice that had developed severe colitis (the severity of colitis was evaluated by measuring the colonic diameter through the laparotomy procedure) were used as previously described (28). The mice receiving local gene delivery were sacrificed at the time points indicated in figure legends. For continuous mucolytic treatment, an ALZET osmotic pump (Alzet Co.) filled with *N*-acetyl-L-cystein was implanted within the dorsa of mice as previously described (52). *N*-acetyl-L-cystein (20 μg/h) was continuously delivered into the cecal lumen for 14 days through a catheter from the implanted osmotic pumps.

Inhibition of IL-22 activity in vivo. For DSS colitis, mice were treated with 3.5% DSS (MP Biomedicals) in drinking water for 5 days, and this treatment was terminated by changing DSS water to normal water. Repeated treatments with anti–IL-22 Abs or control IgG (1.5 mg/injection, 4 times) at days 4, 5, 6, and 7 were performed in selected mice, which showed 3% to 5% of body weight loss at day 4 as compared with initial body weight. In some experiments, local gene delivery with pSecTag2/Hygro vector carrying full-length mouse IL-22BP cDNA was performed in the proximal part of the colon, and the mice were subsequently treated with 3% DSS on the third day after gene delivery. DSS treatment was terminated at day 5 after initiation of DSS treatment, and mice were sacrificed at day 8.

Statistics. Statistical analysis was performed using the Mann-Whitney U test. *P* values of less than 0.05 were considered statistically significant.

Acknowledgments

We would like to thank Daniel K. Podolsky and the Center for the Study of Inflammatory Bowel Disease for kindly providing biopsy samples, Robert Sabat for his critical review of this manuscript, Mari Mino-Kenudson for her useful comments, and Yoh Ishiguro for kindly providing some surgical tissue samples. This study was supported by the Broad Medical Research Program (IBD-0160), the Eli and Edythe L. Broad Foundation; NIH DK64351 (to A. Mizoguchi); NIH DK47677 (to A.K. Bhan); NIH DK44319 (to R.S. Blumberg); and the Center for the Study of Inflammatory Bowel Disease (NIH DK43351). K. Sugimoto was supported by a research fellowship award from the Crohn's and Colitis Foundation of America.

Received for publication July 5, 2007, and accepted in revised form October 31, 2007.

Address correspondence to: Atsushi Mizoguchi, Massachusetts General Hospital, Experimental Pathology Unit, Simches 8234, 185 Cambridge Street, Boston, Massachusetts 02114, USA. Phone: (617) 726-2588; Fax: (617) 726-2365; E-mail: amizoguchi@partners.org.

1. Dumoutier, L., Louahed, J., and Renauld, J.C. 2000. Cloning and characterization of IL-10-related T cell-derived inducible factor (IL-TIF), a novel cytokine structurally related to IL-10 and inducible by IL-9. *J. Immunol.* **164**:1814–1819.
2. Fickenscher, H., et al. 2002. The interleukin-10 family of cytokines. *Trends Immunol.* **23**:89–96.
3. Pestka, S., et al. 2004. Interleukin-10 and related cytokines and receptors. *Annu. Rev. Immunol.* **22**:929–979.
4. Liang, S.C., et al. 2006. Interleukin (IL)-22 and IL-17 are coexpressed by Th17 cells and cooperatively enhance expression of antimicrobial peptides. *J. Exp. Med.* **203**:2271–2279.
5. Zheng, Y., et al. 2007. Interleukin-22, a Th17 cytokine, mediates IL-23-induced dermal inflammation and acanthosis. *Nature.* **445**:648–651.
6. Radaeva, S., Sun, R., Pan, H.N., Hong, F., and Gao, B. 2004. Interleukin 22 (IL-22) plays a protective role in T cell-mediated murine hepatitis: IL-22 is a survival factor for hepatocytes via STAT3 activation. *Hepatology.* **39**:1332–1342.
7. Wolk, K., et al. 2004. IL-22 increases the innate immunity of tissues. *Immunity.* **21**:241–254.
8. Brand, S., et al. 2006. IL-22 is increased in active Crohn's disease and promotes proinflammatory gene expression and intestinal epithelial cell migration. *Am. J. Physiol. Gastrointest. Liver Physiol.* **290**:G827–G838.
9. Nagalakshmi, M.L., Rascle, A., Zurawski, S., Menon, S., and de Waal Malefyt, R. 2004. Interleukin-22 activates STAT3 and induces IL-10 by colon epithelial cells. *Int. Immunopharmacol.* **4**:679–691.
10. Wolk, K., et al. 2006. IL-22 regulates the expression of genes responsible for antimicrobial defense, cellular differentiation, and mobility in keratinocytes: a potential role in psoriasis. *Eur. J. Immunol.* **36**:1309–1323.
11. Andoh, A., et al. 2005. Interleukin-22, a member of the IL-10 subfamily, induces inflammatory responses in colonic subepithelial myofibroblasts. *Gastroenterology.* **129**:969–984.
12. Podolsky, D.K. 2002. Inflammatory bowel disease. *N. Engl. J. Med.* **347**:417–429.
13. Shirazi, T., Longman, R.J., Corfield, A.P., and Probert, C.S.J. 2000. Mucins and inflammatory bowel disease. *Postgrad. Med. J.* **76**:473–478.
14. Targan, S.R., and Karp, L.C. 2005. Defects in mucosal immunity leading to ulcerative colitis. *Immunol. Rev.* **206**:296–305.
15. Yen, D., et al. 2006. IL-23 is essential for T cell-mediated colitis and promotes inflammation via IL-17 and IL-6. *J. Clin. Invest.* **116**:1310–1316.
16. Strober, W., Fuss, I., and Mannon, P. 2007. The fundamental basis of inflammatory bowel disease. *J. Clin. Invest.* **117**:514–521.
17. Wolk, K., et al. 2007. IL-22 induces IL-22 Induces lipopolysaccharide-binding protein in hepatocytes: a potential systemic role of IL-22 in Crohn's disease. *J. Immunol.* **178**:5973–5981.
18. Bhan, A.K., Mizoguchi, E., Smith, R.N., and Mizoguchi, A. 1999. Colitis in transgenic and knockout animals as models of human inflammatory bowel disease. *Immunol. Rev.* **169**:195–207.
19. Mombaerts, P., et al. 1993. Spontaneous development of inflammatory bowel disease in T cell receptor mutant mice. *Cell.* **75**:274–282.
20. Powrie, F. 2004. Immune regulation in the intestine: a balancing act between effector and regulatory T cell responses. *Ann. N. Y. Acad. Sci.* **1029**:132–141.
21. Mizoguchi, E., et al. 2003. Colonic epithelial functional phenotype varies with type and phase of experimental colitis. *Gastroenterology.* **125**:148–161.
22. Steidler, L., et al. 2000. Treatment of murine colitis by *Lactococcus lactis* secreting interleukin-10. *Science.* **289**:1352–1355.
23. Wirtz, S., Becker, C., Blumberg, R., Galle, P.R., and Neurath, M.F. 2002. Treatment of T cell-dependent experimental colitis in SCID mice by local administration of an adenovirus expressing IL-18 antisense mRNA. *J. Immunol.* **168**:4117–4120.
24. Wiethoff, C.M., Smith, J.G., Koe, G.S., and Middaugh, C.R. 2001. The potential role of proteoglycans in cationic lipid-mediated gene delivery. *J. Biol. Chem.* **276**:32806–32813.
25. Sioud, M., and Sorensen, D.R. 2003. Cationic liposome-mediated delivery of siRNAs in adult mice. *Biochem. Biophys. Res. Commun.* **312**:1220–1225.
26. Cryan, S.A., and O'Driscoll, C.M. 2003. Mechanistic studies on nonviral gene delivery to the intestine using in vitro differentiated cell culture models and an in vivo rat intestinal loop. *Pharm. Res.* **20**:569–575.
27. McAlindon, M.E., et al. 1999. Investigation of the expression of IL-1β converting enzyme and apoptosis in normal and inflammatory bowel disease (IBD) mucosal macrophages. *Clin. Exp. Immunol.* **116**:251–257.
28. Mizoguchi, A., Mizoguchi, E., Takedatsu, H., Blumberg, R.S., and Bhan, A.K. 2002. Chronic intestinal inflammatory condition generates IL-10-producing regulatory B cell subset characterized by CD1d upregulation. *Immunity.* **16**:219–230.
29. Jacobs, L.R., and Huber, P.W. 1985. Regional distribution and alterations of lectin binding to colorectal mucin in mucosal biopsies from controls and subjects with inflammatory bowel diseases. *J. Clin. Invest.* **75**:112–118.
30. McCormick, D.A., Horton, L.W., and Mee, A.S. 1990. Mucin depletion in inflammatory bowel disease. *J. Clin. Pathol.* **43**:143–146.

31. Yuan, Z.L., et al. 2004. Central role of the threonine residue within the p+1 loop of receptor tyrosine kinase in STAT3 constitutive phosphorylation in metastatic cancer cells. *Mol. Cell. Biol.* **24**:9390–9400.
32. Chen, Y., et al. 2003. Stimulation of airway mucin gene expression by interleukin (IL)-17 through IL-6 paracrine/autocrine loop. *J. Biol. Chem.* **278**:17036–17043.
33. van der Sluis, M., et al. 2006. Muc2-deficient mice spontaneously develop colitis, indicating that muc2 is critical for colonic protection. *Gastroenterology.* **131**:117–129.
34. Ho, S.B., et al. 2006. Cysteine-rich domains of muc3 intestinal mucin promote cell migration, inhibit apoptosis, and accelerate wound healing. *Gastroenterology.* **131**:1501–1517.
35. Seril, D.N., Liao, J., Ho, K.L., Yang, C.S., and Yang, G.Y. 2002. Inhibition of chronic ulcerative colitis-associated colorectal adenocarcinoma development in a murine model by *N*-acetylcysteine. *Carcinogenesis.* **23**:993–1001.
36. Logsdon, N.J., et al. 2004. The IL-10R2 binding hot spot on IL-22 is located on the N-terminal helix and is dependent on N-linked glycosylation. *J. Mol. Biol.* **342**:503–514.
37. Hokama, A., et al. 2004. Induced reactivity of intestinal $CD4^+$ T cells with an epithelial cell lectin, galectin-4, contributes to exacerbation of intestinal inflammation. *Immunity.* **20**:681–693.
38. Xu, W., et al. 2001. A soluble class II cytokine receptor, IL-22RA2, is a naturally occurring IL-22 antagonist. *Proc. Natl. Acad. Sci. U. S. A.* **98**:9511–9516.
39. Atreya, R., et al. 2000. Blockade of interleukin 6 trans signaling suppresses T-cell resistance against apoptosis in chronic intestinal inflammation: evidence in Crohn's disease and experimental colitis in vivo. *Nat. Med.* **6**:583–588.
40. Takeda, K., et al. 1999. Enhanced Th1 activity and development of chronic enterocolitis in mice devoid of Stat3 in macrophages and neutrophils. *Immunity.* **10**:39–47.
41. Tebbutt, N.C., et al. 2002. Reciprocal regulation of gastrointestinal homeostasis by SHP2 and STAT-mediated trefoil gene activation in gp130 mutant mice. *Nat. Med.* **8**:1089–1097.
42. Welte, T., et al. 2003. STAT3 deletion during hematopoiesis causes Crohn's disease-like pathogenesis and lethality: a critical role of STAT3 in innate immunity. *Proc. Natl. Acad. Sci. U. S. A.* **100**:1879–1884.
43. Corfield, A.P., Carroll, D., Myerscough, N., and Probert, C.S. 2001. Mucins in the gastrointestinal tract in health and disease. *Front. Biosci.* **6**:D1321–D1357.
44. An, G., et al. 2007. Increased susceptibility to colitis and colorectal tumors in mice lacking core 3-derived O-glycans. *J. Exp. Med.* **204**:1417–1429.
45. Mashimo, H., Wu, D.C., Podolsky, D.K., and Fishman, M.C. 1996. Impaired defense of intestinal mucosa in mice lacking intestinal trefoil factor. *Science.* **274**:262–265.
46. McVay, L.D., et al. 2006. Absence of bacterially induced RELMβ reduces injury in the dextran sodium sulfate model of colitis. *J. Clin. Invest.* **116**:2914–2923.
47. Uhlig, H.H., et al. 2006. Differential activity of IL-12 and IL-23 in mucosal and systemic innate immune pathology. *Immunity.* **25**:309–318.
48. Kullberg, M.C., et al. 2006. IL-23 plays a key role in Helicobacter hepaticus-induced T cell-dependent colitis. *J. Exp. Med.* **203**:2485–2494.
49. Duerr, R.H., et al. 2006. A genome-wide association study identifies IL23R as an inflammatory bowel disease gene. *Science.* **314**:1461–1463.
50. Schnyder-Candrian, S., et al. 2006. Interleukin-17 is a negative regulator of established allergic asthma. *J. Exp. Med.* **203**:2715–2725.
51. Matsuo, K., Ota, H., Akamatsu, T., Sugiyama, A., and Katsuyama, T. 1997. Histochemistry of the surface mucous gel layer of the human colon. *Gut.* **40**:782–789.
52. Mizoguchi, A., Mizoguchi, E., and Bhan, A.K. 1999. The critical role of interleukin-4 but not interferon-γ in the pathogenesis of colitis in T cell receptor α mutant mice. *Gastroenterology.* **116**:320–326.

GASTROENTEROLOGY 2007;133:559–573

Lamina Propria c-kit$^+$ Immune Precursors Reside in Human Adult Intestine and Differentiate Into Natural Killer Cells

HIROSHI CHINEN,*,‡ KATSUYOSHI MATSUOKA,* TOSHIRO SATO,* NOBUHIKO KAMADA,* SUSUMU OKAMOTO,* TADAKAZU HISAMATSU,* TAKU KOBAYASHI,* HIROTOSHI HASEGAWA,§ AKIRA SUGITA,¶ FUKUNORI KINJO,‡ JIRO FUJITA,‡ and TOSHIFUMI HIBI*

*Division of Gastroenterology and Hepatology, Department of Internal Medicine, School of Medicine, Keio University, Tokyo, Japan; ‡Department of Medicine and Therapeutics, Control and Prevention of Infectious Diseases, Graduate School of Medicine, University of the Ryukyus, Okinawa, Japan; §Department of Surgery, School of Medicine, Keio University, Tokyo, Japan; and ¶Department of Surgery, Yokohama Municipal Citizen's Hospital, Yokohama, Japan

Background & Aims: **Recent studies have revealed that murine intestinal mucosa contains several kinds of lineage markers (lin)$^-$ c-kit$^+$ immune precursor cells. However, immune precursors in the human adult intestine have not been studied extensively.** ***Methods:*** **Lamina propria mononuclear cells and intraepithelial lymphocytes from surgically resected human adult intestine were examined for the surface antigen expression and cytokine profile by immunohistochemistry and flow cytometry. The transcriptional profile of these cells was analyzed by reverse-transcription polymerase chain reaction. The phenotypic and functional characterization of the in vitro differentiating cells from the precursors was examined by flow cytometry.** ***Results:*** **We identified lin$^-$ c-kit$^+$ cells scattered throughout lamina propria of the human adult intestine. These intestinal immune precursors expressed CD34, CD38, CD33, interleukin-2Rα, and interleukin-7Rα, and they had much more abundant expression of Id2, PU.1, SpiB1, and lymphotoxin than thymocytes. The lin$^-$ c-kit$^+$ immune precursors mainly differentiated into CD56$^+$ c-kit^{dim} cells during in vitro culture. These in vitro differentiating cells corresponded to intestinal natural killer (NK) cells, which had distinct characteristics from their peripheral counterparts, such as CD83 and integrin α_E expression, less cytotoxic activity, and higher interferon-γ production. Furthermore, both c-kit^{dim} cells and NK cells were increased in lamina propria of Crohn's disease, although there was no change for peripheral blood NK cells.** ***Conclusions:*** **The human intestine may have the unique NK cell differentiation system, which may contribute to maintenance of immune homeostasis in the intestine.**

The cellular components of the immune system, such as T cells, B cells, monocytes, granulocytes, macrophages, dendritic cells, and natural killer (NK) cells, are derived from common hematopoietic stem cells (HSCs) in the bone marrow. As a first step, HSCs differentiate into 2 distinct subsets: common myeloid progenitors and common lymphoid progenitors. Although common myeloid progenitors ultimately differentiate into myeloid cells such as monocytes, granulocytes, macrophages, and dendritic cells,[1] common lymphoid progenitors differentiate into B-cell precursors and common T- and NK-cell precursors (T/NKPs).[2] T/NKPs subsequently differentiate into NKPs and T-cell precursors.[3–5] These steps are assumed to proceed mainly in the bone marrow, which is regarded as the most important site for primary immune cell differentiation.

A unique immune system has developed in the intestine. The intestinal immune system includes Peyer's patches, isolated lymphoid follicles, mesenteric lymph nodes (MLN), lamina propria mononuclear cells (LPMCs), and intraepithelial lymphocytes (IELs). This intestinal immune system maintains immunologic homeostasis against gut luminal antigens. In addition to these components, the intestine has become recognized as a site for differentiation of immune cells. Recent studies have revealed that murine intestinal mucosa contains immune precursor cells, which are lymphoid tissue inducer cells (LTi)[6,7] in the fetus and cryptopatch (CP) cells[8] in the adult. Both LTi and CP cells express c-kit, IL-7 receptor α subunit (IL-7Rα), IL-2Rα, CD44, and CD4^{dim}. These surface phenotypes are similar to those of common lymphoid progenitors in bone marrow, and LTi and CP cells have been reported to develop in situ into Peyer's patches[6,7,9] and extrathymic T cells of IELs,[10,11] respectively. In addition, a recent study suggested that CP cells can function as adult LTi by developing into isolated lymphoid folli-

Abbreviations used in this paper: CP, cryptopatch; HSC, common hematopoietic stem cell; IENK, intraepithelial natural killer cell; IFN, interferon; IL, interleukin; IL-7Rα, IL-7 receptor α subunit; Lin, lineage markers; LPMCs, lamina propria mononuclear cells; LPNKs, lamina propria natural killer cells; LTi, lymphoid tissue inducer cells; MLN, mesenteric lymph nodes; NK, natural killer; PBL, peripheral blood lymphocytes; PBNKs, peripheral blood natural killer cells; PCR, polymerase chain reaction; pTα, pre-T cell receptor chain α; RAG, recombination activating gene; SEM, standard error of the mean; T/NKPs, common T and natural killer cell precursors; TNF, tumor necrosis factor.

0016-5085/07/$32.00
doi:10.1053/j.gastro.2007.05.017

cles rather than IELs in normal adult mice.[12] The immune precursor cells in the murine intestine have been investigated extensively; however, only a few reports have referred to immune precursor cells in the human intestine. A recent study showed that $CD3^-$ $CD7^+$ cells in the human fetal intestine express messenger RNA (mRNA) for pre-T-cell receptor chain α (pTα), which is essential for early T-cell differentiation.[13] It also shows that these cells can give rise to $CD3^+$ T cells in vitro and in vivo, using severe combined immunodeficient (SCID) mice engrafted with human fetal intestine.[14] It also has been reported that recombination activating gene (RAG)-1 and RAG-2 mRNA can be detected in the intestinal mucosa of human infants.[15,16] Moreover, $CD3^-$ $CD2^+$ $CD7^+$ cells in the human adult jejunum have been shown to express RAG mRNA as well as pTα mRNA.[16] All these reports have examined intestinal immune precursors in light of extrathymic T-cell differentiation. However, considering the reports on the murine intestine, we assume that more immature immune precursor cells, such as LTi, also may reside in the human adult intestine.

To verify this hypothesis, we first analyzed human adult intestine immunohistochemically, focusing on expression of c-kit, which is a receptor for stem cell factor and is known to be expressed on immune precursor cells such as HSCs.[17] Although intensive analysis did not reveal any $c\text{-}kit^+$ cell clusters such as CP, we found a considerable number of $c\text{-}kit^+$ cells scattered in the lamina propria. We next characterized with flow cytometry these $c\text{-}kit^+$ cells in LPMCs isolated from human adult intestine, which revealed that the $c\text{-}kit^+$ cells in the intestine have phenotypes identical to T/NKPs in the fetal liver[18] and thymus.[19] The $c\text{-}kit^+$ cells mainly were committed to the NK cell lineage in vitro. We also found unique characteristics of mature NK cells residing in the human adult intestine. These results suggest that $c\text{-}kit^+$ cells should differentiate into intestinal NK cells. Furthermore, NK cell differentiation is accelerated in Crohn's disease (CD), indicating that this intestinal NK cell differentiation system may play a role in the pathogenesis of chronic intestinal inflammation. Thus, we were able to show differentiation of intestinal NK cells from $c\text{-}kit^+$ cells in the human adult intestine, which may contribute to maintenance of intestinal immune homeostasis.

Materials and Methods

Tissue Samples

Normal intestinal mucosa and MLN were obtained from macroscopically and microscopically unaffected areas of patients with colon cancer. Intestinal mucosa also was obtained from surgically resected specimens from patients with CD or ulcerative colitis (UC), diagnosed on the basis of clinical, radiographic, endoscopic, and histologic findings, according to established criteria.[20,21] In all samples from patients with CD or UC, the degree of inflammation was histologically moderate to severe. All experiments were approved by the institutional review board and written informed consent was obtained from all the patients.

Histologic Analysis

Tissue sections were treated according to well-established methods. Intestinal specimens were fixed with 4% paraformaldehyde (Wako Pure Chemical Industries, Osaka, Japan) and embedded in paraffin. Sections from paraffin-embedded blocks were deparaffinized and stained with H&E (Sakura Finetech Japan, Tokyo, Japan). For immunohistochemical staining, deparaffinized sections were heated at 100°C for 20 minutes in 10 mmol/L sodium citrate buffer (pH 6.0) in a microwave oven. For the enzyme-labeled antibody method, each section was treated with 3% H_2O_2 (Wako) in 100% methanol and then incubated with normal rabbit serum (Nichirei Biosciences, Tokyo, Japan) for 15 minutes at room temperature to block nonspecific reactions. Thereafter, sections were treated with rabbit anti-human c-kit Ab (Dako Cytommation, Glostrup, Denmark) and incubated at 4°C overnight. Primary antibodies were washed out and sections were incubated with Histofine anti-rabbit Simplestain Max-PO (Nichirei), and visualized with 3-3′-diaaminobenzidine (Nichirei) for peroxidase and counterstained with hematoxylin. Sections incubated with the IgG fraction of normal rabbit serum (Dako) served as negative controls. For identification of mast cells, deparaffinized sections were stained with .05% toluidine blue solution, pH 4.1 (Wako). Mast cells were stained red-purple and other cells were stained blue.

Preparation of LPMCs, IELs, Peripheral Blood Lymphocytes (PBLs), and MLN Cells

LPMCs and IELs were isolated from intestinal specimens using modifications of previously described techniques.[22,23] Briefly, dissected mucosa was incubated in calcium and magnesium-free Hanks' balanced salt solution (Sigma-Aldrich, St. Louis, MO) containing 2.5% heat-inactivated fetal bovine serum (BioSource, Camarillo, CA) and 1 mmol/L dithiothreitol (Sigma-Aldrich) to remove mucus. The mucosa then was incubated in Hanks' balanced salt solution containing 1 mmol/L ethylenediaminetetraacetic acid (EDTA) (Sigma-Aldrich) for 60 minutes at 37°C. During this treatment, IELs and epithelial cells were removed from the tissue. Tissues were collected and incubated in Hanks' balanced salt solution containing .02% collagenase type 3 (Worthington Biochemical, Freehold, NJ) for 60 minutes at 37°C. The fraction was pelleted and resuspended in 40% Percoll solution (Amersham Biosciences, Piscataway, NJ), then layered on 60% Percoll before centrifugation at 2000 rpm for 20 minutes at room temperature. Viable LPMCs were recovered from the 40%–60% layer interface. For isolation of IELs, after EDTA treatment the supernatants were

collected and filtered through a glass-wool column to deplete cell debris and sticky cells. Cells were centrifuged over a 40%–60% Percoll solution density gradient. IELs were recovered from the layer interface. PBLs were isolated from heparinized peripheral blood samples by density gradient centrifugation using Lymphoprep (Nycomed Pharma, Oslo, Norway). For isolation of MLN cells, MLN were squeezed and passed through sterile nylon mesh to create single-lymphocyte suspensions.[24]

Giemsa Stain

The lin$^-$ c-kit$^+$ cells and the mast cells in LPMCs were sorted by Epics Altra with the HyPerSort cell sorting system (Beckman-Coulter, Fullerton, CA). The purity of the sorted cells was greater than 98% by postsorting analysis. After spreading the sorted cells on glass slides they were air dried, then the cells were fixed with methanol and stained with pH 6.4 Giemsa solution (Merck, Whitehouse Station, NJ), and they were observed by light microscope.

Flow Cytometric Analysis of c-kit$^+$ LPMCs Differentiation Markers

Cell surface fluorescence intensity was assessed using a FACSCalibur analyzer and analyzed with Cell Quest software (BD Biosciences, San Jose, CA). Dead cells were excluded with propidium iodide staining. The lineage marker monoclonal antibodies that were used were the available Lineage Cocktail 1 (BD Biosciences). Lineage Cocktail 1 included CD3 (SK7), CD14 (MϕP9), CD16 (3G8), CD19 (SJ25C1), CD20 (L27), and CD56 (NCAM16.2). All the antibodies were purchased from BD Biosciences except for CD2, CD20, CD56 (MEM188), and NKG2D, which were purchased from eBiosciences (San Diego, CA); CCR7, CXCR5, and IL-18Rα were purchased from R&D systems (Minneapolis, MN); CD133 was purchased from Miltenyi Biotec (Bergisch, Gladbach, Germany); and CX3CR1 was purchased from Medical & Biological Laboratories (Nagoya, Japan).

Quantitative Real-Time, Reverse-Transcription Polymerase Chain Reaction Analysis

Cells were sorted by Epics Altra with the HyPerSort cell sorting system (Beckman-Coulter). The purity of the sorted cells was always greater than 98% by postsorting analysis. Total RNA was extracted using the RNeasy Micro Kit (Qiagen, Hilden, Germany), and total thymocyte RNA was purchased from BD Biosciences. Total RNA was treated with Qiagen DNase I to remove any contaminating genomic DNA. Absence of amplification of contaminating genomic DNA was ascertained by polymerase chain reaction (PCR) in which RNA was used as a template. Complementary DNA was synthesized using the Superscript first-strand synthesis system for reverse-transcription PCR (Invitrogen, Carlsbad, CA), according to the manufacturer's instructions. Semiquantitative real-time, reverse-transcription PCR was performed using TaqMan universal PCR master mix (Applied Biosystems, Foster City, CA) and on-demand gene-specific primers. The fluorogenic probes were as follows: RAG-1, RAG-2, preTCRα, Id2, PU.1, SpiB1, lymphotoxin α, lymphotoxin β, and β-actin, which all were purchased from Applied Biosystems. Cycling conditions for PCR amplification were 95°C for 10 minutes, followed by 45 cycles of 94°C for 15 seconds, and 60°C for 1 minute. Transcription of mRNA was assessed on a DNA Engine Opticon 2 System and analyzed with Opticon monitor software (MJ Research, Waltham, MA). All samples were analyzed in triplicate.

Lin$^-$ c-kit$^+$ LPMCs In Vitro Culture

CD3$^+$ and CD56$^+$ cells were removed from LPMCs using a magnetic cell-sorting system (MACS; Miltenyi Biotec) according to the manufacturer's instructions. The CD3$^-$ CD56$^-$ LPMCs were cultured at a concentration of 1×10^6/mL in complete medium consisting of 1640 RPMI (Sigma-Aldrich) supplemented with GlutaMAX (Invitrogen), 10% heat-inactivated fetal bovine serum (BioSource), 10 mmol/L HEPES (Invitrogen), 50 μmol/L 2-mercaptoethanol (Wako), 100 U/mL penicillin, and 100 mg/mL streptomycin (Invitrogen). The cultures were maintained in a humidified atmosphere at 37°C in 5% CO_2 for 72 hours. All samples were cultured in duplicate.

Isolation of Peripheral Blood NK Cells and Lamina Propria NK Cells

CD56^{dim} (CD3$^-$ CD14$^-$ CD16$^+$ CD56$^+$) peripheral blood NK (PBNK) cells and CD56^{bright} (CD3$^-$ CD14$^-$ CD16$^-$ CD56$^+$) PBNKs were isolated from PBLs by using MACS (Miltenyi Biotec) according to the manufacturer's instructions. Lamina propria NK (LPNK) cells (CD3$^-$ CD14$^-$ CD56$^+$) also were isolated with MACS. The percentage of each isolated NK cell was evaluated by flow cytometry and routinely was greater than 95%.

Cytotoxicity Assay

The cytotoxicity of NK cell subsets against the NK-sensitive K562, a human erythroleukemic cell line (American Type Culture Collection, Rockville, MD), was measured by using a previously described protocol[25] with minor modifications.

NK Cell Cytokine Production

A total of 1×10^6 cells in 1 mL complete RPMI 1640 medium (Sigma-Aldrich) were stimulated with 10 ng/mL IL-12 (Medical & Biological Laboratories) and 100 ng/mL IL-15 (R&D) or 10 ng/mL IL-12 (Medical & Biological Laboratories) and 100 ng/mL IL-18 (Medical & Biological Laboratories) for 8 hours at 37°C. After stimulation, interferon-γ (IFN-γ) or tumor necrosis factor-α

(TNF-α) production were detected using the Cytokine Secretion Assay Cell Detection Kit (Miltenyi Biotec) according to the manufacturer's instructions, defining cells with antibodies against CD3, CD56, or CD117 (BD Biosciences) and propidium iodide. IFN-γ and TNF-α in cell culture supernatant also were measured using human Th1/Th2 cytokine beads array kit (BD Biosciences) according to the manufacturer's protocol.

Transplantation of the Human lin⁻ c-kit⁺ LPMCs Into RAG-2⁻/⁻ Mice

C57BL/6J background RAG-2$^{-/-}$ mice (Central Institute for Experimental Animals, Kanagawa, Japan) were housed under specific pathogen-free conditions at the animal center of Keio University (Tokyo, Japan). All experiments using mice were approved by and performed according to the guidelines of the animal committee of Keio University. The human lin⁻ c-kit⁺ LPMCs cells ($1.3–1.5 \times 10^5$) were injected intraperitoneally into 8-week-old RAG-2$^{-/-}$ mice. LPMCs, IELs, and splenic lymphocytes were isolated and examined for human lineage markers and human CD117 monoclonal antibody (BD Biosciences) by flow cytometry. For in vitro differentiation, isolated LPMCs were cultured with complete medium in the presence of 100 U/mL human recombinant IL-2 (eBiosciences) or 100 ng/mL IL-15 (R&D) for 7 days. Cultured cells were stained by human CD3 and CD56 monoclonal antibody (BD Biosciences) and assessed by flow cytometry. All samples were cultured in duplicate.

Statistical Analysis

Statistical analysis was performed by using STATVIEW software version J-5.0 (Abacus Concepts, Berkeley, CA), StatMate III software version 3.05 (ATMS, Tokyo, Japan), and GraphPad Prism software version 4.0 (GraphPad Software Inc., San Diego, CA). Differences at a P value of less than .05 were considered significant. All data are expressed as means ± standard error of the mean (SEM).

Results

Presence of Non–Cluster-Forming Lineage Markers (lin)⁻ c-kit⁺ Lymphocytes in the Human Adult Intestine

We first tried to identify c-kit⁺ cells in the human adult intestine by immunohistochemistry. We could not find any c-kit⁺ cell clusters such as murine CP cells; however, we found a considerable number of c-kit⁺ cells scattered in the intraepithelial space, lamina propria, and submucosal layers of both the ileum and colon (Figure 1*A* and *B*). The c-kit expression on IELs was dimmer than that on LPMCs (Figure 1*B* and *I*). Furthermore, the c-kit⁺ IELs were found only in the intraepithelial space of crypts, but not in that of villi (data not shown). Because c-kit also is expressed on mast cells,[26] sequential sections were stained metachromatically with toluidine blue, which is useful for identifying mast cells (Figure 1*C*). Although most of the c-kit⁺ cells in the submucosal layer and a part of the c-kit⁺ cells in the lamina propria presented metachromasia (Figure 1*G* and *H*), a considerable proportion of the c-kit⁺ LPMCs and IELs did not (Figure 1*E*, *F*, *I*, and *J*). We next analyzed with flow cytometry LPMCs isolated from human adult intestine. Mast cells were excluded by taking advantage of their complex granular morphology and higher c-kit expression[27] (Figure 2*A*). The other c-kit⁺ population, distinct from mast cells, was consistent with a typical lymphoid cell gate in forward- and side-scatter diagrams and was used for further analysis. We then examined these c-kit⁺ cells for lineage markers as follows: CD3, CD14, CD16, CD19, CD20, and CD56. The blot diagram clearly identified 2 distinct c-kit⁺ populations: lin⁻ c-kit⁺ and lin⁺ c-kit^{dim} cells (Figure 2*B*). The lin⁻ c-kit⁺ subset occupied 1.97% ± .15%, whereas the lin⁺ c-kit^{dim} subset occupied 1.29% ± .22% of the total LPMCs (n = 10). The lin⁻ c-kit⁺ cells were different from mast cells morphologically, and they seemed to be small immature lymphoid cells about 7 μm in diameter (Figure 2*C*). A similar number of lin⁻ c-kit⁺ cells were detected in LPMCs from both the ileum and colon; however, they barely were recognized in IELs, MLN cells, or PBLs (Figure 2*B*). In contrast, the lin⁺ c-kit^{dim} subset also was present in IELs, which was consistent with the immunohistochemical finding that c-kit expression on IELs was dimmer than that on LPMCs (Figure 1*B* and *I*). We assumed that these lin⁻ c-kit⁺ cells were immune precursor cells in the intestine.

Characterization of the lin⁻ c-kit⁺ and lin⁺ c-kit^{dim} Subsets

To characterize further the 2 c-kit⁺ populations in LPMCs, we examined the expression of various surface stem cell markers. The lin⁻ c-kit⁺ cells also expressed CD34 (Figure 3*A*), which is another marker for HSCs.[28] However, CD34 expression on lin⁻ c-kit⁺ cells was lower than that on HSCs (Figure 3*A*). It is reported that the expression of CD34 decreases during differentiation, therefore, lower CD34 expression may reflect a later stage in the hematopoietic lineage.[29] The lin⁻ c-kit⁺ cells in LPMCs expressed CD38^{dim}, Thy-1, and CD45RA (Figure 3*A*), which corresponds to the phenotype of T/NKPs in fetal liver[18] and thymus.[19] Furthermore, they expressed IL-7Rα, IL-2Rα, CD44, CCR7, and CXCR5 (Figure 3*B*), which are expressed on immune precursor cells such as mouse LTi and CP cells. Importantly, a small number of the lin⁻ c-kit⁺ cells in LPMCs expressed IL-2Rβ and CD161, which are known as NK cell markers (Figure 3*B*). The lin⁻ c-kit⁺ cells were negative for CD56 when examined with clone NCAM 16.2 and MEM 188; however, a small fraction of the cells were weakly positive for clone B159. It is interesting to note that this subset expressed CD33, a known marker of myeloid lineage cells (Figure 3*A* and *B*).[30]

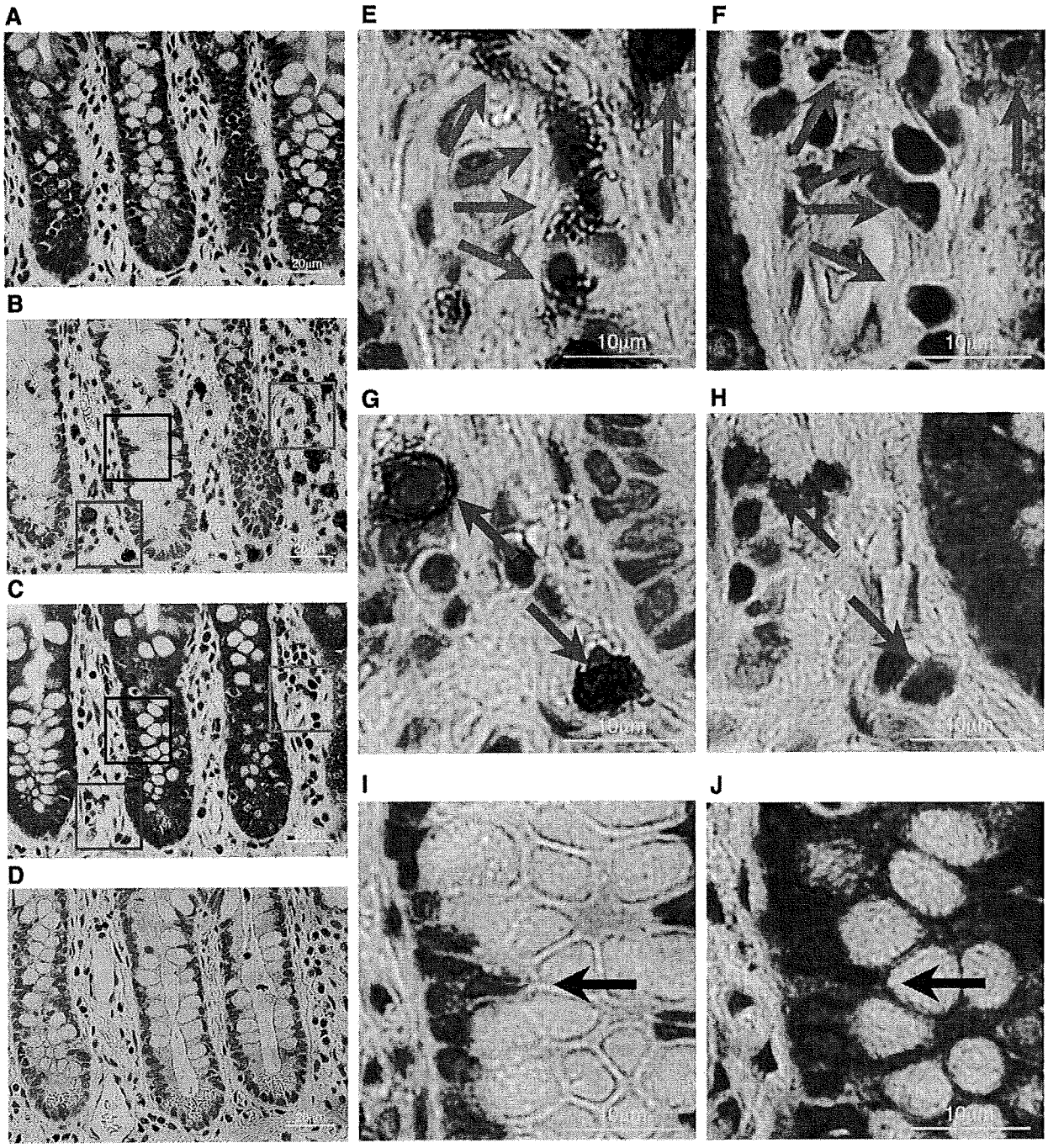

Figure 1. Identification of c-kit–expressing cells in the human adult intestine. Sequential sections of ileal mucosa were stained with (*A*) H&E, (*B*) c-kit antibody by 3-3′-diaaminobenzidine–enhanced immunoperoxidase and counterstained with hematoxylin, (*C*) toluidine *blue* to identify mast cells, and (*D*) negative control. The high-power image of representative c-kit$^+$ cells (*G*, *H*) with metachromatic staining (*red frame*) or (*E*, *F*) without metachromatic staining (*blue frame*) metachromatic staining. The high-power image of a (*I*) representative c-kit$^+$ IEL without metachromatic staining is shown in the (*J*) *black frame*.

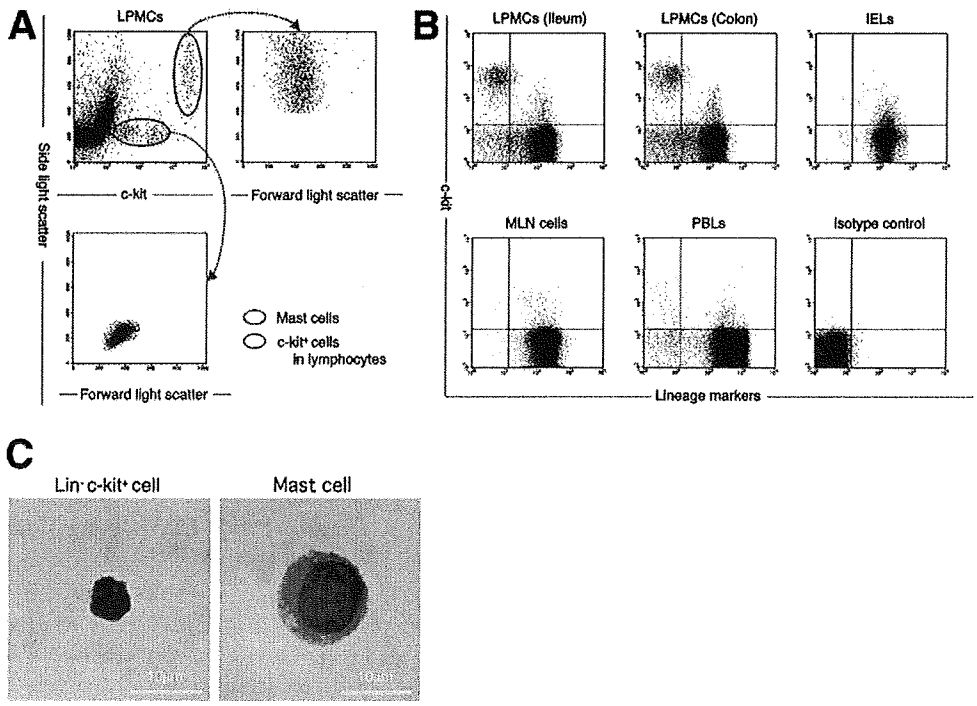

Figure 2. Flow cytometry of lin$^-$ c-kit$^+$ subset of LPMCs isolated from human adult intestine. (*A*) LPMCs were highlighted with c-kit expression and side-light scatter blotting (*upper left*). Side-light scatter high and c-kit high cells (red oval), which represented mast cells, were expanded further with side- and forward-side–scatter blotting (*upper right*). The cells with lower c-kit expression and lower side light scatter (*blue oval*) were expanded with the side- and forward-side–scatter blotting (*bottom left*). These cells were within a typical lymphoid cell gate. (*B*) LPMCs from ileum or colon, IELs, PBLs, and MLN cells in the lymphoid gate were analyzed for expression of c-kit and lineage markers (CD3, CD14, CD16, CD19, CD20, and CD56). The data shown are representative of 6 independent experiments. (*C*) The lin$^-$ c-kit$^+$ cells and the mast cells from LPMCs were stained with Giemsa solution.

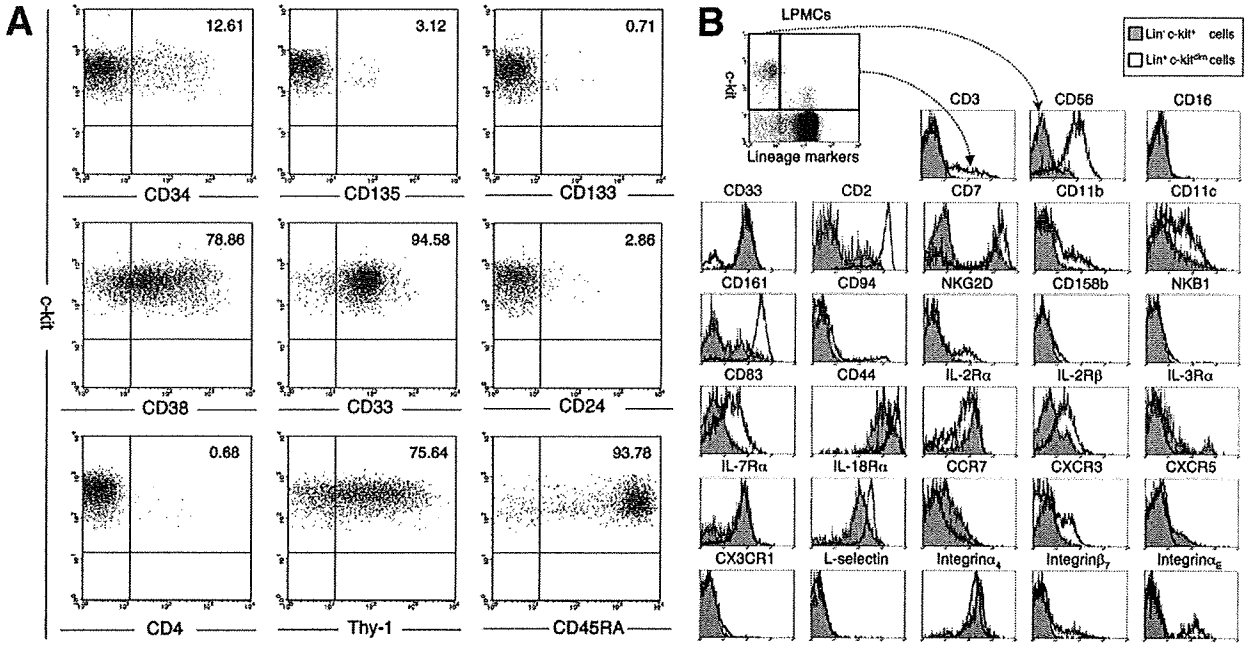

Figure 3. Characterization of the lin$^-$ c-kit$^+$ and lin$^+$ c-kit^{dim} subsets of LPMCs. (*A*) Stem cell marker expression was analyzed in the lin$^-$ c-kit$^+$ subset of LPMCs. (*B*) The lin$^-$ c-kit$^+$ subset (*gray histograms*) and the lin$^+$ c-kit^{dim} subset (*black lines*) of LPMCs were analyzed for the expression of several cell surface antigens. The data shown are representative of at least 5 experiments for each surface marker.

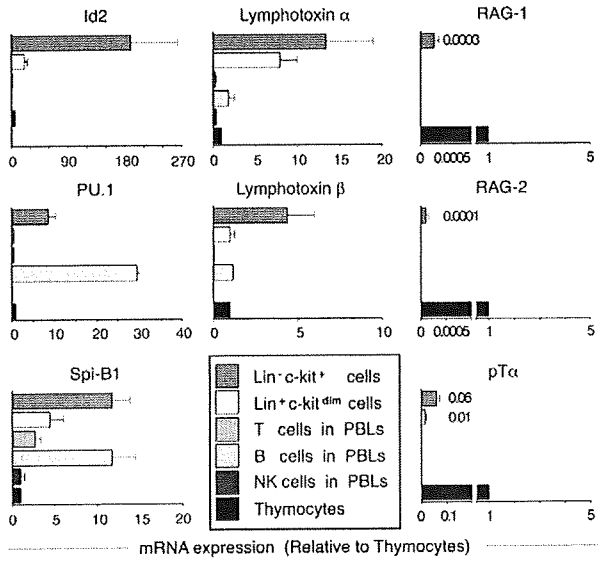

Figure 4. The lin⁻ c-kit⁺ subset has abundant mRNA for Id2, PU.1, SpiB1, and lymphotoxin α and β mRNA transcripts for each gene were quantified using real-time reverse-transcription PCR. In each sample, mRNA transcripts were normalized to those of β-actin. The expression value of each mRNA is shown as a ratio against that of thymocytes. Peripheral T, B, and NK cells were used as controls. Results are expressed as means ± SEM. The data are representative of 4 samples.

We next analyzed the lin⁺ c-kit^{dim} subset in LPMCs (Figure 3*B*). The lin⁺ c-kit^{dim} cells expressed only CD3 and CD56 among the lineage markers, and CD56⁺ cells predominated over CD3⁺ cells. The lin⁺ c-kit^{dim} subset also expressed other NK markers, IL-2Rβ and CD161, and these phenotypes corresponded to those of NKPs.[31,32] Interestingly, they expressed CD83 (Figure 3*B*), but they did not express other dendritic cell markers such as CD80, CD86, and CD209 (data not shown). It was also an intriguing finding that a fraction of these cells expressed integrin α_E, known as an IEL marker (Figure 3*B*).[33]

With the surface antigen expression patterns, the lin⁻ c-kit⁺ cells in the LPMCs were reminiscent of T/NKPs. On the other hand, the lin⁺ c-kit^{dim} subset likely may be a group of cells that already have begun differentiation into NK cells.

The lin⁻ c-kit⁺ Subset Has Abundant mRNA for Id2, PU.1, SpiB1, and Lymphotoxin

To confirm further the immature nature and differentiation potential of the lin⁻ c-kit⁺ cells, we examined the mRNA expression of several transcription factors essential for HSC differentiation. PU.1 and SpiB1 play important roles in HSC differentiation[34,35] and Id2 is essential for NK cell development.[36] The lin⁻ c-kit⁺ cells had much more abundant expression of Id2, PU.1, and SpiB1 mRNA compared with thymocytes (Figure 4). Note that mRNA of these transcription factors was decreased in the lin⁺ c-kit^{dim} cells, suggesting that they were at a later stage of differentiation than the lin⁻ c-kit⁺ population.

In addition to these transcription factors, we analyzed lymphotoxin α and β mRNA transcripts. Lymphotoxin α and β are reported to be critical for both NK cell development[37] and fulfillment of LTi functions.[38] The lin⁻ c-kit⁺ cells also had much more abundant mRNA transcripts of lymphotoxin α and β compared with thymocytes (Figure 4).

We next examined RAG-1, RAG-2, and pTα mRNA, which are essential for early T-cell differentiation. Although these transcripts were detectable in the lin⁻ c-kit⁺ cells, their expressions were far lower than that in thymocytes (Figure 4). These results indicate that the lin⁻ c-kit⁺ cells have an immature nature and the potential to differentiate into NK cells.

The lin⁻ c-kit⁺ LPMCs Are Committed to NK Cell Lineage In Vitro

Based on the results obtained so far, we assumed that the lin⁻ c-kit⁺ cells in the human adult intestine were a subset very close to T/NKPs. To confirm the differentiation capacity of the lin⁻ c-kit⁺ cells, we cultured LPMCs after depletion of both CD3⁺ and CD56⁺ cells without any exogenous stimuli. This culture method can maintain the interaction of the c-kit⁺ cells with the surrounding cells, via cell–cell contact or humoral soluble factors, which may be essential for the differentiation process. At the beginning of the culture period, we confirmed that the lin⁺ c-kit^{dim} subset was excluded completely because of CD3⁺ and CD56⁺ cell depletion (Figure 5*A*). However, surprisingly, c-kit^{dim} cells expressing lineage markers emerged and increased during the culture period (Figure 5*A* and *B*). Conversely, the lin⁻ c-kit⁺ cells gradually decreased. These lin⁺ c-kit^{dim} cells must have developed from the lin⁻ c-kit⁺ subset because the c-kit^{dim} cells did not emerge from the sorted c-kit⁻ population during 72 hours of culture (Supplementary Figure 1; supplementary material online at www.gastrojournal.org).

The c-kit⁺ cells became larger in size and had more granularity as they developed (Figure 5*C*). Most of the c-kit^{dim} cells up-regulated NK cell markers such as CD56, CD161, and IL-2Rβ, and they also expressed integrin α_E (Figure 5*C*, *D*, and *E*, Table 1). However, they did not express activated NK cell markers CD80 and CD86 (Table 1).[39] Meanwhile, very few CD3⁺ cells could be detected among the lin⁺ c-kit^{dim} populations (Figure 5*C* and *D*). Furthermore, the CD56⁺ cells in the newly emerging lin⁺ c-kit^{dim} cells contained cytotoxic granules (Figure 5*F*) and they could exert cytotoxicity against K562 cells (Figure 5*G*). They also were able to produce IFN-γ and TNF-α (Figure 5*H*). According to some previous studies, it takes up to 2 weeks for NK cell development from HSC in vitro culture.[40] Therefore, the lin⁻ c-kit⁺ subset likely included the population that already committed to NK cell lineage.

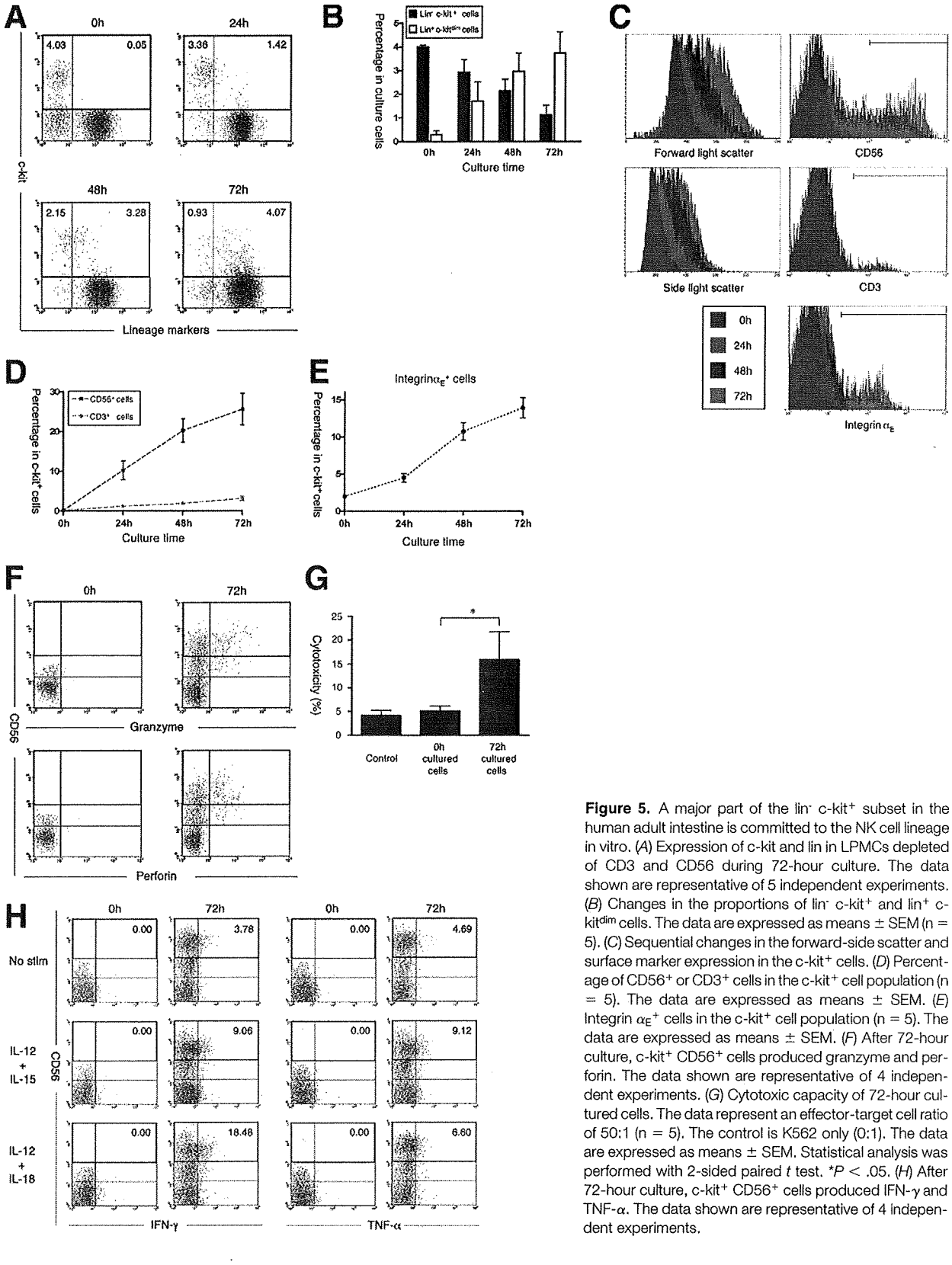

Figure 5. A major part of the lin⁻ c-kit⁺ subset in the human adult intestine is committed to the NK cell lineage in vitro. (*A*) Expression of c-kit and lin in LPMCs depleted of CD3 and CD56 during 72-hour culture. The data shown are representative of 5 independent experiments. (*B*) Changes in the proportions of lin⁻ c-kit⁺ and lin⁺ c-kit^{dim} cells. The data are expressed as means ± SEM (n = 5). (*C*) Sequential changes in the forward-side scatter and surface marker expression in the c-kit⁺ cells. (*D*) Percentage of CD56⁺ or CD3⁺ cells in the c-kit⁺ cell population (n = 5). The data are expressed as means ± SEM. (*E*) Integrin α_E⁺ cells in the c-kit⁺ cell population (n = 5). The data are expressed as means ± SEM. (*F*) After 72-hour culture, c-kit⁺ CD56⁺ cells produced granzyme and perforin. The data shown are representative of 4 independent experiments. (*G*) Cytotoxic capacity of 72-hour cultured cells. The data represent an effector-target cell ratio of 50:1 (n = 5). The control is K562 only (0:1). The data are expressed as means ± SEM. Statistical analysis was performed with 2-sided paired *t* test. *$P < .05$. (*H*) After 72-hour culture, c-kit⁺ CD56⁺ cells produced IFN-γ and TNF-α. The data shown are representative of 4 independent experiments.

Table 1. Phenotypes of the Newly Emerging c-kit^{dim} Cells After 72-Hour In Vitro Culture

Cell surface markers	Cultured cells (72 h)
CD34	–
CD38	+++
CD33	++
CD2	+++
CD7	++
CD11b	+
CD11c	+
CD161	+++
CD94	+
NKG2D	+
CD158a/b	–
NKB1	–
L-selectin	–
CD80	–
CD83	+
CD86	–
CD209	–
IL-2Rα	++
IL-2Rβ	++
IL-3Rα	–/+
IL-7Rα	+++
IL-18Rα	+++
CCR7	+
CXCR3	+
CXCR5	–
CX3CR1	–
Integrin α_4	+++
Integrin β_7	+
Integrin α_E	+

–, 0%–5%; –/+, 5%–10%; +, 10%–50%; ++, 50%–75%; +++, 75%–100%.

When only isolated lin$^-$ c-kit$^+$ cells were rendered to in vitro culture, they lost viability with or without exogenous human cytokines such as IL-2 and/or IL-15. Then we performed transfer experiments in which RAG-2–deficient mice received isolated human lin$^-$ c-kit$^+$ LPMCs. Very surprisingly, 3 weeks after transplantation we could detect human lin$^-$ c-kit$^+$ cells exclusively in murine LPMCs but not in IELs or splenic lymphocytes (Figure 6*A*). The absence of CD56 expression indicated that they did not differentiate into NK cells in murine intestine. However, human CD56$^+$ cells emerged when murine LPMCs containing human lin$^-$ c-kit$^+$ cells were cultured with exogenous IL-2 and/or IL-15 (Figure 6*B*).

These results suggested that a large proportion of human LP lin$^-$ c-kit$^+$ cells were the NK cell precursors. Given that newly emerging lin$^+$ c-kit^{dim} cells from lin$^-$ c-kit$^+$ subtype shared a very similar phenotype with the lin$^+$ c-kit^{dim} cells that actually reside in human LPMCs (Figure 3B and Table 1), this differentiation process may actually occur in the human intestine.

LPMCs and IELs Contain Functional NK Cells

The results thus far have indicated that the lin$^-$ c-kit$^+$ cells in the intestine have the potential to differentiate into NK cells. There have been only a few reports on NK cells in the human intestine,[41,42] therefore, we examined CD56 expression on LPMCs and IELs. It revealed that a considerable number of CD3$^-$ CD56$^+$ cells certainly exist in LPMCs (Figure 7*A*). These CD3$^-$ CD56$^+$ cells, which are referred to as LPNKs, were larger and had more granular morphology than lamina propria T cells (Supplementary Figure 2; supplementary material online at www.gastrojournal.org). CD3$^-$ CD56$^+$ cells also were found in IELs, which are referred to as intraepithelial NK cells (IENKs) (Figure 7*A*).[42] We next compared surface marker expression among the lin$^-$ c-kit$^+$, lin$^+$ c-kit^{dim}, and intestinal NK cells (LPNKs and IENKs) (Figure 7*B*). NK cell markers such as CD94, CD161, and NKG2D increased in the following order: lin$^-$ c-kit$^+$ cells < lin$^+$ c-kit^{dim} cells < intestinal NK cells, which is consistent with CD56 up-regulation on lin$^+$ c-kit^{dim} cells. Conversely, immature cell markers such as c-kit, IL-7Rα, and CD33 were decreased in the same order. These changes in surface marker expression also were observed during differentiation of lin$^-$ c-kit$^+$ cells into lin$^+$ c-kit^{dim} cells (Table 1). Taken together, these results would support the hypothesis that lin$^-$ c-kit$^+$ cells differentiate into intestinal NK cells via lin$^+$ c-kit^{dim} cells, possibly at the site of the intestine.

It is known that PBNK cells can be divided into 2 subsets according to the intensity of CD56 expression: CD56^{dim} and CD56^{bright} NK cells.[43,44] Although CD56 expression on the intestinal NK cells was not as high as on CD56^{bright} NK cells, the intestinal NK cells were reminiscent of CD56^{bright} NK cells owing to the lack of CD16, CX3CR1, and killer cell inhibitory receptor (CD158a/b, NKB1) expression (Figure 7*B*).[45,46] Moreover, both the intestinal NK cells and the peripheral CD56^{bright} NK cells expressed CD33, whereas the peripheral CD56^{dim} NK cells did not (Figure 7*B*).

To confirm that the intestinal NK cells harbor NK functions, cytotoxic molecules were examined. Both LPNKs and IENKs contained granzyme and perforin; and they were equipped with cytotoxic function, although the activity was weaker than that in peripheral CD56^{dim} NK cells (Figure 7*C* and *D*). Both LPNKs and IENKs also produced IFN-γ and TNF-α at a level comparable with peripheral CD56^{bright} NK cells (Figure 7*E–H*). With these phenotypes (ie, lower expression of granzyme and perforin and higher IFN-γ and TNF-α production), intestinal NK cells are reminiscent of peripheral CD56^{bright} NK cells. However, they clearly were discriminated from peripheral CD56^{bright} NK cells in terms of CD83 and integrin α_E expression (Figure 7*B*). These unique characteristics of intestinal NK cells may support the idea that they may have an original in situ differentiation system independent from PBNKs.

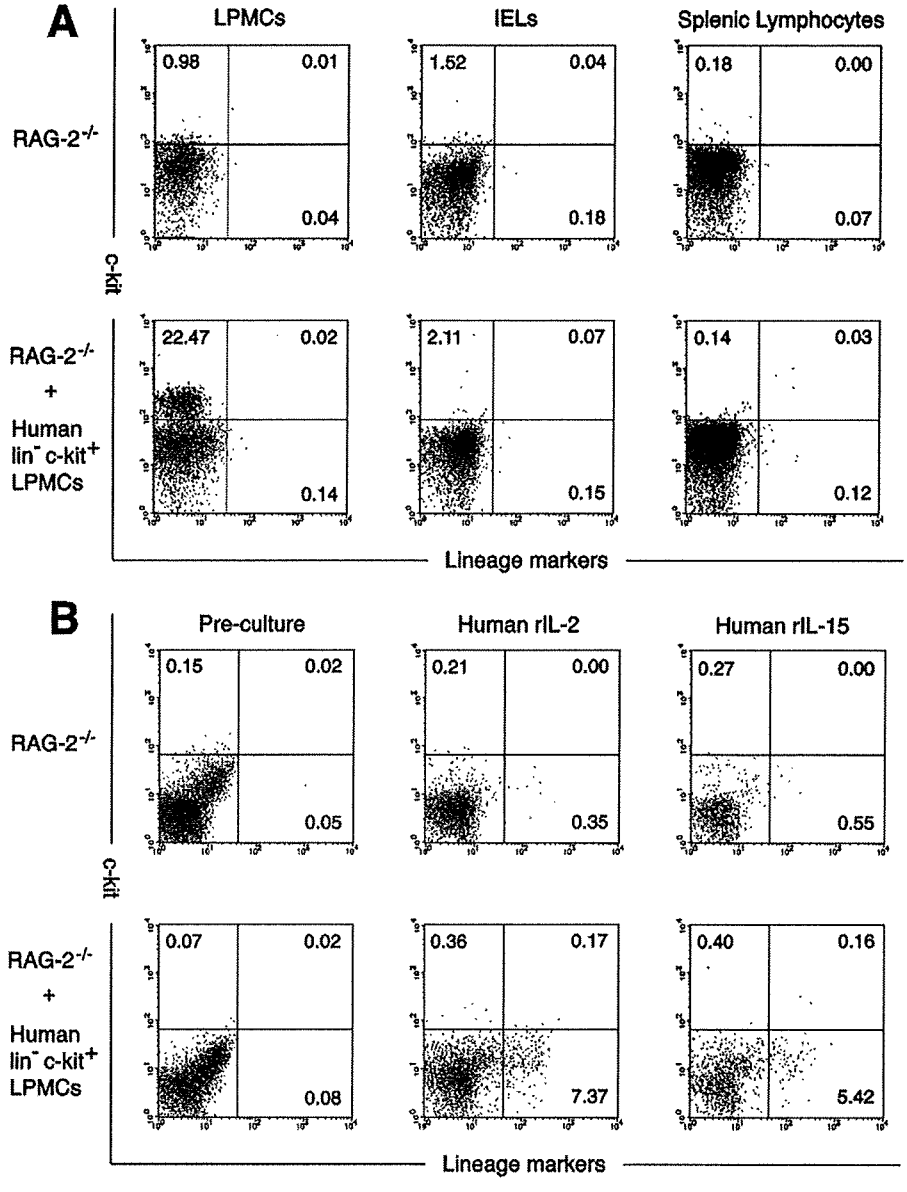

Figure 6. Human lin⁻ c-kit⁺ LPMCs after the transfer into recipient mice could differentiate into NK cells. (*A*) LPMCs, IELs, and splenic lymphocytes isolated from the RAG$^{-/-}$ mice transplanted with human lin⁻ c-kit⁺ LPMCs were stained by lineage markers and CD117 monoclonal antibody and were analyzed by fluorescence-activated cell sorter. The data shown are representative of 2 independent experiments. (*B*) Isolated LPMCs were cultured with human recombinant IL-2 (rIL-2) or rIL-15 for 7 days. The cultured cells were analyzed for expression of human CD3 and CD56. The data shown are representative of 2 independent experiments.

Intestinal NK Cells Are Increased in CD, Reflecting Accelerated Differentiation of lin⁻ c-kit⁺ Cells Into NK Cells

The involvement of NK cells in intestinal inflammation has not been well documented. Therefore, we examined intestinal NK cells in inflammatory bowel disease, a chronic inflammatory condition that consists of 2 major forms: CD and UC.[47] Flow cytometry revealed that both LPNKs and IENKs were increased in the samples from CD but not from UC patients, compared with

Figure 7. Analysis of surface antigen expression and function of intestinal NK cells. (*A*) LPMCs, IELs, and PBLs were stained for CD3 and CD56. CD3⁻ CD56⁺ cells were examined further for c-kit expression. (*B*) Expression of various surface markers, including NK cell markers, was compared among lin⁻ c-kit⁺ and lin⁺ c-kit^{dim} cells, LPNKs, IENKs, and PBNKs. The data shown are representative of more than 4 cases for each surface marker. (*C*) Production of granzyme, perforin from LPNKs, IENKs, and PBNKs were determined with intracellular staining. The data shown are representative of 4 independent experiments. (*D*) Cytotoxicity of freshly isolated LPNKs (n = 5) and PBNKs (n = 4). Effector-target ratio was 10:1. The data were expressed as means ± SEM. (*E*) IFN-γ and (*F*) TNF-α production from LPNKs (n = 5) and PBNKs (n = 4) after 72-hour culture with indicated cytokines. The data were expressed as means ± SEM. (*G*) IFN-γ or (*H*) TNF-α production in LPNKs, IENKs, and PBNKs after 8 hours of cytokine stimulation were detected using the Cytokine Secretion Assay Cell Detection Kit (Miltenyi Biotec). The data shown are representative of 4 independent experiments.

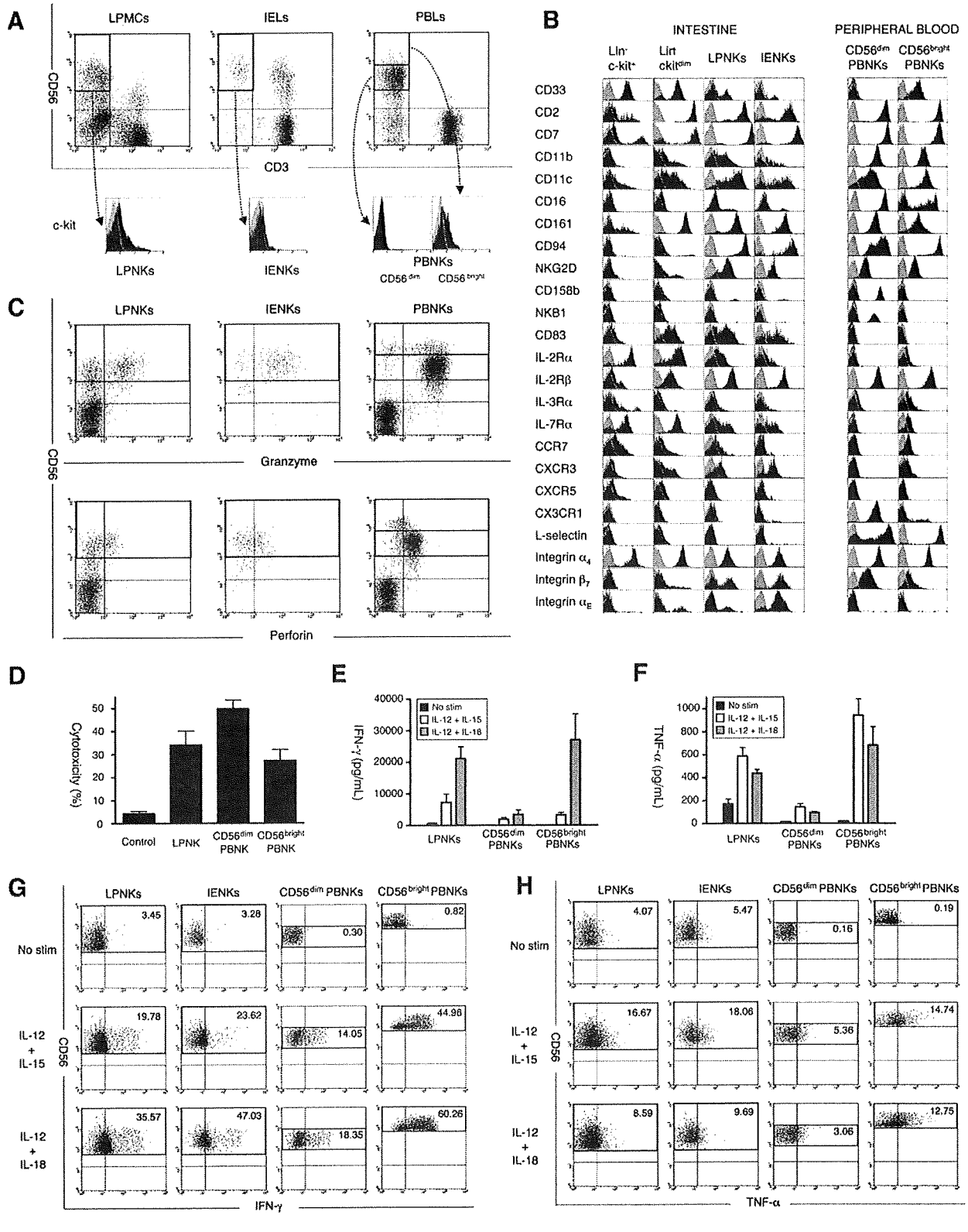
A
LPMCs
IELs
PBLs
CD56
CD3
c-kit
LPNKs
IENKs
PBNKs
CD56dim CD56bright
B
INTESTINE
PERIPHERAL BLOOD
Lin- c-kit+
Lin- ckitdim
LPNKs
IENKs
CD56dim PBNKs
CD56bright PBNKs
CD33
CD2
CD7
CD11b
CD11c
CD16
CD161
CD94
NKG2D
CD158b
NKB1
CD83
IL-2Rα
IL-2Rβ
IL-3Rα
IL-7Rα
CCR7
CXCR3
CXCR5
CX3CR1
L-selectin
Integrin α4
Integrin β7
Integrin αE
C
LPNKs
IENKs
PBNKs
CD56
Granzyme
Perforin
D
Cytotoxicity (%)
Control
LPNK
CD56dim PBNK
CD56bright PBNK
E
IFN-γ (pg/mL)
No stim
IL-12 + IL-15
IL-12 + IL-18
LPNKs
CD56dim PBNKs
CD56bright PBNKs
F
TNF-α (pg/mL)
No stim
IL-12 + IL-15
IL-12 + IL-18
LPNKs
CD56dim PBNKs
CD56bright PBNKs
G
LPNKs
IENKs
CD56dim PBNKs
CD56bright PBNKs
No stim
IL-12 + IL-15
IL-12 + IL-18
CD56
IFN-γ
3.45
3.28
0.30
0.82
19.78
23.62
14.05
44.98
35.57
47.03
18.35
60.26
H
LPNKs
IENKs
CD56dim PBNKs
CD56bright PBNKs
No stim
IL-12 + IL-15
IL-12 + IL-18
CD56
TNF-α
4.07
5.47
0.16
0.19
16.67
18.06
5.36
14.74
8.59
9.69
3.06
12.75